https://doi.org/10.5194/egusphere-2026-1335
Preprint. Discussion started: 18 March 2026

Integrating Ozone–vegetation Damage Schemes into SSiB4/TRIFFID: Evaluation of Six Parameterizations and Refinement of Ozone Decay Process Across Plant Functional Types

Lingfeng Li[1], Bo Qiu[1,2], Siwen Zhao[1], Xin Miao[1], Chaorong Chen[1], Jiuyi Chen[1], Yueyang Ni[1], Xin Huang[1,2], Haishan Chen[3,4], Weidong Guo[1]

[1]School of Atmospheric Sciences, Nanjing University, Nanjing, 210023, China
[2]Frontiers Science Center for Critical Earth Material Cycling, Nanjing University, Nanjing, 210023, China.
[3]School of Atmospheric Sciences, Nanjing University of Information Science and Technology, Nanjing, 210044, China
[4]State Key Laboratory for Climate System Predictions and Risk Management/Key Laboratory of Meteorological Disaster, Ministry of Education/Collaborative Innovation Center on Forecast and Evaluation of Meteorological Disasters, Nanjing University of Information Science and Technology, Nanjing, 210044, China

Correspondence to: Bo Qiu (qiubo@nju.edu.cn)

Abstract. Tropospheric ozone (O_3) is a major air pollutant that threatens vegetation productivity and terrestrial ecosystems. Quantifying O_3-induced impacts on photosynthesis and stomatal conductance is crucial for understanding biosphere-atmosphere interactions at regional and global scales. In recent decades, several parameterization schemes have been developed to describe the photosynthetic and stomatal responses to O_3 exposure. However, substantial discrepancies remain when applying different schemes in various model frameworks. In this study, we integrated six flux-based O_3-vegetation damage parameterizations into SSiB4/TRIFFID, a well-established dynamic global vegetation model, to assess the impacts of O_3 pollution on vegetation photosynthesis in China during the 2010s. Our results indicate that O_3 pollution led to approximately a 20% reduction in GPP during the 2010s, with discrepancies ranging from 15% to 31% across different schemes. Comparison of the O_3 damage schemes revealed substantial differences in plant O_3 sensitivity across schemes and plant functional types (PFTs). When evaluated against observations, the newly developed L2024 parameterization—which features non-linear response formulations—and the trait-informed approaches based on leaf mass per area (LMA) both reproduce observed O_3 sensitivity more closely, as reflected in their consistently smaller biases. This improved performance can be attributed to the inclusion of a broader range of observational and experimental data, as well as key physiological parameters (e.g., LMA) to better capture O_3 sensitivity. Furthermore, we found that the L2024 scheme exhibited strong inhibition of photosynthesis in the late growing season due to cumulative O_3 exposure. By refining the "decay" process of O_3 accumulation using leaf lifespan parameters and applying the "decay" and "healing" processes across all PFTs, we improved the spatial and temporal distribution of gross primary productivity (GPP) simulations. This study highlights the importance of observations and physiological insights in developing O_3-vegetation damage parameterizations. Future efforts should focus on expanding observational and experimental data on O_3 responses in China's natural ecosystems to enhance O_3 damage assessment and model development.

https://doi.org/10.5194/egusphere-2026-1335
Preprint. Discussion started: 18 March 2026

1 Introduction

Tropospheric ozone (O_3) is a secondary air pollutant formed through the photochemical oxidation of carbon monoxide (CO), methane (CH_4), volatile organic compounds (VOCs), and nitrogen oxides (NOx) in the presence of sunlight (Wang et al., 2022). As a short-lived climate forcer and a phytotoxic air pollutant, O_3 concentrations have risen substantially since pre-industrial times, driven by increasing emissions of its precursors from fossil fuel combustion and industrial activities (Long et al., 2024; Lu et al., 2018; Li et al., 2021). As a result, current tropospheric O_3 levels are estimated to be approximately 40% higher than pre-industrial concentrations in many mid-latitude regions of the Northern Hemisphere (Tarasick et al., 2019; Turnock et al., 2020). In recent decades, rapid economic development and industrialization in China have driven a marked increase in surface O_3 concentrations, making China a prominent hotspot for O_3 pollution globally (Lu et al., 2018; Li et al., 2021). The elevated surface O_3 in China poses severe threats to both public health and terrestrial ecosystems (Ainsworth et al., 2012; Monks et al., 2015; Agathokleous et al., 2020). Given the significant ecological impacts, systematically quantifying the effects of O_3 on vegetation in China is essential for understanding its broader impacts on regional carbon uptake and climate change (Liu et al., 2025; Zhou et al., 2024).

Controlled fumigation and field exposure experiments are crucial for advancing our knowledge of O_3 effects on vegetation. Observation evidences consistently show that elevated O_3 reduces photosynthesis and biomass, with significant variability in plant functional type sensitivity (Wittig et al., 2007; Emberson, 2020; Cheesman et al., 2024). Diffusion of O_3 fluxes through stomata triggers the formation of reactive oxygen species (ROS), leading to oxidative stress that damages photosynthetic activity, disrupts stomatal function, accelerates senescence, and reduces plant biomass accumulation (Grulke and Heath, 2020). In response, plants have evolved efficient antioxidant systems to counteract ROS and mitigate oxidative damage through various repair processes (Castagna and Ranieri, 2009; Li et al., 2017). Experimental evidence has provided valuable insights into the impacts of O_3 on vegetation. However, much of the existing evidence comes from site-level studies, which is derived from artificially controlled open-top chamber (OTC) experiments rather than natural ambient O_3 exposures. Moreover, due to the uncertainties arising from extrapolating beyond experimental conditions, the limited spatial coverage of site observations makes it challenging to accurately assess O_3-induced vegetation damage at regional scales (Liu et al., 2024; Cao et al., 2024).

Alternatively, mechanistic parameterizations were proposed and implemented in numerical models as a feasible approach to quantify O_3-induced vegetation damage across regional to global scales. Currently, three major flux-based frameworks for ozone-vegetation damage have been developed and integrated into dynamic vegetation models (Sitch et al., 2007; Lombardozzi et al., 2015; Ma et al., 2023). Sitch et al. (2007) established a semi-mechanistic scheme (hereafter S2007) to describe the O_3 impacts on photosynthesis as a function of instantaneous stomatal ozone flux, and the stomata response is calculated based on the coupling between stomatal conductance and leaf photosynthesis. This scheme was later implemented by Yue and Unger (2014) into the Yale Interactive terrestrial Biosphere (YIBs) model and estimated a 14% of net primary productivity (NPP) loss due to surface O_3 pollution in China (Yue et al., 2017). On the other hand, Lombardozzi et al. (2015) proposed a new scheme (hereafter L2015) based on cumulative uptake of ozone (CUO), in which ozone effects on photosynthesis and stomatal

https://doi.org/10.5194/egusphere-2026-1335
Preprint. Discussion started: 18 March 2026

conductance are described by independent response functions. Incorporation of L2015 scheme into Community Land Model (CLM) indicated an 8–12% decline in gross primary productivity (GPP) globally, with localized reductions exceeding 20% over hotspot regions such as eastern United States, western Europe, and eastern China. In addition to the approaches above, Ma et al. (2023) introduced leaf mass per area (LMA) to construct a trait-based O_3 damage parameterization within the S2007 framework. The implementation of LMA unifies the representation of area-based plant sensitivities to ozone across global grids, thereby replacing the prescribed PFT-specific ozone sensitivity parameters in previous frameworks with a single, mass-based constant. Using this scheme, Ma et al. (2023) estimated a contemporary global mean reduction of 4.8% in GPP, with large reductions (>10%) occurring in the eastern US and eastern China.

Overall, numerous parameterizations have been proposed to quantify the O_3-indced vegetation damage in land surface models. However, despite the ongoing advances in O_3 damage parameterizations, large inter-scheme discrepancies persist in the simulated vegetation responses. These discrepancies are particularly critical in China, where severe O_3 pollution, coupled with the urgent need for effective policy-making to mitigating its effects, highlights the need for accurate simulation of O_3-induced vegetation losses. Previous studies using different models and parameterizations have reported a large spread in O_3-induced GPP reductions ranging from -4% to -40% in China (Yue et al., 2017; Xie et al., 2019; Zhu et al., 2022; Jin et al., 2023; Cao et al., 2024). Such divergence reflects the discrepancies in simulation periods, model framework, and scheme selection, which underscores considerable uncertainties in current evaluations of O_3 impacts. Moreover, several recently developed parameterizations, including the new scheme in CLM proposed by (Li et al., 2024), the re-calibrated S2007 scheme by (Ma et al., 2023), and the abovementioned LMA-based approach, have not been comprehensively evaluated within regional simulations for China. These uncertainties and research gaps underscore the need for long-term, systematic inter-scheme comparisons in ozone-vegetation damage simulations. In this study, we address these gaps by conducting an intercomparison of six mechanistic O_3 damage parameterizations within the well-established SSiB4/TRIFFID land surface model. Using this unified model framework, we quantify the O_3-induced vegetation damage in China through a decade-long simulation of the 2010s. We then assess the inter-scheme discrepancies and evaluate each parameterization against observed dose-response relationships from fumigation experiments in peer-reviewed literatures. Finally, we refine the representation of cumulative O_3 uptake and update the parameters with trait observations. These modifications alleviate the overestimation of O_3 damage and improve the spatial distribution and seasonality of GPP simulations.

https://doi.org/10.5194/egusphere-2026-1335
Preprint. Discussion started: 18 March 2026

2 Material and Methods

2.1 SSiB4/TRIFFID model

The Simplified Simple Biosphere Model version 4 coupled with the Top-down Representation of Interactive Foliage and Flora Including Dynamics Model (SSiB4/TRIFFID) is used in this study to investigate the response of terrestrial ecosystems to stomatal uptake of O_3. SSiB4/TRIFFID is a process-based land surface model integrated with dynamic global vegetation model. The model is designed to simulate the energy, water, and carbon cycles at the terrestrial surface, incorporating well-established mechanisms for calculating multi-timescale vegetation dynamics and land surface characteristics including vegetation cover and structure (Zhang et al., 2015; Liu et al., 2019). The photosynthesis and stomatal processes are based on the framework developed by Collatz et al. (1991) and incorporated by Zhan et al. (2003), with a leaf-to-canopy scaling strategy introduced by Sellers et al. (1996). To date, SSiB4/TRIFFID employs 7 plant function types (PFTs) including evergreen broadleaf forest (EBF), evergreen needleleaf forest (ENF), deciduous broadleaf forest (DBF), shrubland (Shrub), C3 grassland (C3), C4 grassland (C4), and tundra (Tundra) (Liu et al., 2019). In this study, all of the SSiB4/TRIFFID simulations are conducted at a spatial resolution of 1°×1° spatial resolution and a temporal interval of 3 hours.

2.2 Parameterization schemes for ozone-vegetation damage

Six O_3 vegetation damage schemes were implemented to SSiB4/TRIFFID, including: (1) the Lombardozzi et al. (2015) scheme used in CLM4.5 (hereafter L2015), (2) Li et al. (2024) scheme applied in CTSM 2.2 (hereafter L2024), (3) the Sitch et al. (2007) scheme used in MOSES (hereafter S2007), (4) re-calibrated S2007 method by Ma et al. (2023) (hereafter CS2007), (5) LMA-based approach by Ma et al. (2023) using gridded global LMA map (hereafter LMAgrid), and (6) prescribed PFT-specific LMA values (hereafter LMApft). All of these schemes are developed based on the stomatal uptake of O_3 flux, a widely accepted approach in the quantification of O_3-induced vegetation damage (Reich, 1987; Karlsson et al., 2007; Gruenhage et al., 2018; Pleijel et al., 2022). The generalized formations for instantaneous stomatal O_3 flux f_{O3} $(nmol\ m^{-2}\ s^{-1})$ and cumulative O_3 uptake POD_y are calculated as follows:

$$PODy = \int \max(f_{O3} - y, 0) \quad (1)$$

$$f_{O3} = \frac{[O_3]}{r + k_{O3} \times r_s} \quad (2)$$

where $[O_3]$ is the O_3 concentration at the top of the canopy, r denotes the aerodynamic and boundary layer resistance between leaf surface and the reference level, k_{O3} is the ratio of leaf resistance for O_3 relative to that for water vapor (1.67), and r_s refers to the stomata conductance for H_2O $(m\ s^{-1})$.The POD_y (phototoxic O_3 dose over a flux threshold of $y\ nmol\ O_3 m^{-2} s^{-1}$) represents the cumulative O_3 uptake at leaf surface This flux-based metric is widely used in risk assessments, given its clear biophysical interpretation and strong linkage to O_3-induced vegetation damage (Pleijel et al., 2022).

https://doi.org/10.5194/egusphere-2026-1335
Preprint. Discussion started: 18 March 2026

Base on the definition of POD_y, Lombardozzi et al. (2015) compiled experimental data from the peer-reviewed literature and formulated photosynthetic and stomatal responses to chronic O_3 exposure as standardized functions of cumulative uptake of ozone (CUO). The L2015 scheme applies separate O_3-damage functions to describe O_3 impacts on photosynthesis and stomatal conductance. The O_3-modification factors on photosynthesis rate (FO3_A) and the stomata conductance (FO3_g) are calculated as:

$$F_{O3\_A} = a_p + b_p \times CUO \tag{3}$$

$$F_{O3\_g} = a_g + b_g \times CUO \tag{4}$$

According to Lombardozzi et al. (2015), the value of CUO at time step t is calculated as:

$$CUO_t = CUO_{t-1}(1 - D) + U(1 - H) \tag{5}$$

Where U represents the instantaneous stomatal O_3 uptake at time step t over the threshold of y ($nmol\ O_3\ m^{-2}s^{-1}$), D represents the decay factor (0 to 1, unitless) of CUO_{t-1} parameterized as a function of the time step length Δt (s) and leaf longevity l_{leaf} (year). H is the healing factor (0 to 1, unitless) derived by leaf area index (LAI) at current and previous timestep, which represents the assumption that newly formed leaves are free of ozone damage initially.

$$U = \max(f_{O3} - y, 0) \tag{6}$$

$$D = \begin{cases} \dfrac{\Delta t}{l_{leaf} \times 3600 \times 24 \times 365}, & evergreen \\ 0, & else \end{cases} \tag{7}$$

$$H = \max\left(1 - \frac{LAI_{t-1}}{LAI_t}, 0\right) \tag{8}$$

Based on a greatly expanded database of O_3 fumigation experiments (approximately six times larger data that used in the L2015 scheme) collected from peer-reviewed literature, Li et al. (2024) developed the L2024 scheme and implemented it in CLM5. According to their estimation, the newly-developed scheme accurately captures the observed responses of photosynthetic rate and stomatal conductance to POD_y across a variety of PFTs. Key formulations and parameter settings for L2015 and L2024 schemes as implemented in SSiB4/TRIFFID are detailed in Table S1.

The S2007 scheme adopt a semi-mechanistic parameterization to represent the transient O_3-induced damage to plants through the coupling between stomatal conductance and photosynthetic rate (Sitch et al., 2007). The O_3-midification factor on photosynthesis (F) is formulated as a function of the instantaneous stomatal O_3 flux exceeding a PFT-specific threshold of y:

$$F_{O3} = 1 - \alpha_{PFT} \times \max(f_{O3} - y, 0) \tag{9}$$

where α_{PFT} is the PFT-specific O_3 sensitivity coefficient derived from observations (Sitch et al., 2007). The coupled formulation of Eq. (2) and Eq. (9) produces a quadratic in F_{O3} that can be solved analytically at each timestep. F_{O3} is then applied as a reduction factor on net photosynthetic rate, while stomatal conductance is subsequently calculated using the semi-empirical Ball-Berry formulation driven by the O_3-modified photosynthetic rate (Collatz et al., 1991; Zhan et al., 2003). Within the same framework, Ma et al. (2023) re-calibrated the sensitivity parameters of S2007 using observed O_3 response relationships derived from field experiments, this re-calibrated version is denoted as CS2007 in this study. Table S1

https://doi.org/10.5194/egusphere-2026-1335
Preprint. Discussion started: 18 March 2026

summarizes the SSiB4/TRIFFID implementation of S2007 and CS2007 scheme, and the sensitivity parameters settings are show in Table S2. More details of the two schemes are provided in Sitch et al. (2007) and Ma et al. (2023).

Motivated by the S2007 framework, Ma et al. (2023) proposed a trait-based parameterization in which the ozone sensitivity of plants is expressed using leaf mass per area. The LMA metric enables mass-based sensitivity representation and uses a single PFT-independent parameter a (a cross-species constant) to unify the ozone sensitivity across different plant species.

$$a = \alpha_{PFT} \times LMA \tag{10}$$

Based on LMA, the O_3 modification factor F_{O3} in Eq. (9) is converted as

$$F_{O3} = 1 - a \times \max\left(\frac{f_{O3}}{LMA} - x, 0\right) \tag{11}$$

Using LMA, the vegetation ozone sensitivity is unified with the new PFT-independent constant a ($nmol^{-1}\ s\ g$), and the flux threshold is reformulated as a mass-based value x ($nmol\ g^{-1}\ s^{-1}$). Following Feng et al. (2018), we set $x = 0.019$ based on the observations. Following Ma et al. (2023), we implement LMAgrid scheme using the global LMA map from Moreno-Martínez et al. (2018) and LMApft scheme using prescribed PFT-specific LMA values (Table S2). Details of the LMA dataset and processing are described in Sect. 2.3.2.

2.3 Simulations

2.3.1 Site-level simulations

To assess the performance of the implemented ozone-damage parameterizations, we perform site-level simulations at two eddy-covariance flux tower sites: Harvard Forest, United States (US-Ha1) (Munger et al., 1996); and Hyytiälä Forest, Finland (FI-Hyy) (Keronen et al., 2003). Currently, continuous, long-term observations of stomatal O3 uptake and carbon fluxes remain scarce in China, particularly for natural ecosystems under ambient ozone exposure. We therefore use US-Ha1 and FI-Hyy as benchmarks before conducting regional simulations over China.

US-Ha1 is a temperate deciduous broadleaf forest with long-term ozone and carbon fluxes measurements available for 1990-2000. FI-Hyy represents a boreal evergreen needleleaf forest dominated by Scots pine (*Pinus sylverstris*), with ozone and carbon fluxes available for 2001-2013. The meteorological forcing, O_3 concentration and flux measurements were aggregated to 3-hourly resolution to match the model timestep. Missing values within 6 hours were filled using the nearest timesteps, while gaps longer than 6 hours were filled using a moving-window (15-day and 3-year windows) at the same hour of day. Years with remaining discontinuities after gap filling were excluded to ensure the continuous ozone input. As a result, we select 1998-1999 for US-Ha1 and 2008-2009 for FI-Hyy as the longest continuous periods.

We conduct six experiments to evaluate the simulated stomatal O_3 uptake and GPP fluxes across the implemented parameterizations (Table 1). These include one control experiment without ozone impacts (O3OFF) and five simulations that applies L2015, L2024, S2007, CS2007, LMApft, respectively. At the site scale, we use LMApft to represent the LMA-based approach, whereas LMAgrid is evaluated in the regional simulations with gridded LMA forcing. The O_3-induced vegetation damage is quantified as the difference between each simulation and the O3OFF experiment.

https://doi.org/10.5194/egusphere-2026-1335
Preprint. Discussion started: 18 March 2026

Table 1. Summary of site-level simulations.

Scheme	Site (Year)
O3OFF	US-Ha1 (1998–1999)
L2015	
L2024	
S2007	FI-Hyy (2008–2009)
CS2007	
LMApft	

2.3.2 Regional simulations over China

We conduct seven experiments to quantify the impacts of ambient O_3 on GPP over China (Table 2). All simulations are performed for 2005–2020 with meteorological forcing from ERA5-Land (Muñoz Sabater, 2019), and the first six years (2005–2010) are discarded as spin-up. For all experiments except O3OFF, ambient O_3 concentrations are derived from the Hourly Surface Ozone Data (HrSOD). HrSOD is an observation-constrained, machine learning-based gridded product that provides hourly surface O_3 at a spatial resolution of 0.1° × 0.1°, which can well capture the spatiotemporal variability of surface ozone pollution over China (Zhang et al., 2024). We further evaluated HrSOD against China's ground-level O_3 monitoring network from the China National Environmental Monitoring Center (CNEMC) (Fig. S1). The results show that HrSOD reproduces the observed spatial pattern of annual-mean O_3 across China for 2015-2020 (R^2=0.71; MAE=9.12μg m^{-3}). In this study, both HrSOD and ERA5-Land forcings are aggregated to 1° and 3-hourly to match the SSiB4/TRIFFID configuration.

For the LMAgrid experiment, we derive gridded LMA product from Moreno-Martínez et al. (2018) as input data for mass-based O_3 damage scheme. Following Ma et al. (2023), we filled the missing LMA values using the global mean value of the corresponding PFT. The gap-filled LMA data is then aggregated to a spatial resolution of 1° to match the model configuration (Fig. S2).

In addition to the seven experiments described above, we performed an additional simulation in which the cumulative ozone uptake (CUO) treatment in L2024 was refined (hereafter $L2024_{modify}$). In the original implementation, the decay term was applied only to evergreen PFTs. Here we extend the decay-healing representation to all PFTs to provide a consistent representation of ozone damage memory and recovery across vegetation types. This modification is conceptually aligned with the framework proposed by Felzer et al. (2009), who represented ozone damage as a prognostic state variable governed by a balance between injury and recovery processes. In their framework, recovery comprises two components: (i) a characteristic healing rate indicating gradual physiological repair, and (ii) a rapid healing associated with canopy growth, whereby newly formed leaves replace the damaged foliage as LAI increases. In $L2024_{modify}$, we extend the decay-healing representation with a similar logic. The decay factor D represents the gradual loss of accumulated O_3 injury related to physiological processes,

https://doi.org/10.5194/egusphere-2026-1335
Preprint. Discussion started: 18 March 2026

while the healing factor H represents the dilution of prior damage associated with LAI increasements. By extending this decay–healing framework consistently to all PFTs, we ensure that both evergreen and deciduous vegetation are allowed to moderate ozone damage through turnover and recovery processes.

$$D = \frac{\Delta t}{l_{leaf} \times 3600 \times 24 \times 365} \quad (12)$$

$$H = \max\left(1 - \frac{LAI_{t-1}}{LAI_t}, 0\right) \quad (13)$$

Furthermore, to better constrain the decay process for all PFTs, we update the key parameter l_{leaf} using observed leaf longevity dataset (Wang et al., 2012). Leaf longevity is a key plant trait that controls typical leaf life span of each PFT, which provides important physiological constraint for representing vegetation turnover in land surface models (Wang et al., 2012; Zhang et al., 2016). By linking the decay term to a measurable physiological trait, this refinement provides a clear representation of chronic O_3 injury and avoids unrealistic accumulation of O_3 damage during the growing season.

Table 2. Summary of regional simulations.

Scheme	Region/Period
O3OFF	China 2005–2020
L2015	
L2024	
S2007	
CS2007	
LMAgrid	
LMApft	

2.4 Benchmark data for model validation

For regional-scale model evaluation over China, we used independent satellite- and data-driven products of leaf area index (LAI) and gross primary productivity (GPP) to assess the simulated vegetation dynamics. For LAI, we obtain the Global Land Surface Satellite (GLASS) LAI product, which is generated using general regression neural networks and remote-sensing observations. Compared to other long-term LAI products, the GLASS LAI is characterized by high accuracy and temporal stability (Liang et al., 2021). In this study, the original GLASS LAI data at 0.05 for 2011–2020 were aggregated to 1° to validate and evaluate the SSiB4/TRIFFID simulations.

We used the GOSIF and FLUXCOM GPP product as independent benchmarks to evaluate the simulated GPP over China. GOSIF GPP is a satellite-based product derived from the Orbiting Carbon Obsevatory-2 (OCO-2) solar-induced chlorophyll fluorescence (SIF) data using a light-use-efficiency framework. GOSIF GPP provides seamless global estimates at 0.05° resolution since 2000 (Li and Xiao, 2019). The FLUXCOM RS+METEO GPP product is derived using machine-learning

https://doi.org/10.5194/egusphere-2026-1335
Preprint. Discussion started: 18 March 2026

approaches that integrates eddy-covariance carbon flux measurements with satellite remote sensing and meteorological data, which is available at 0.5° resolution for 1979-2018 (Jung et al., 2020). We obtain GOSIF and FLUXCOM GPP data from 2011 to 2020 (2018 for FLUXCOM) and interpolate these products to a spatial resolution of 1° to match the model configuration. Both of the datasets have been widely applied in regional and global assessments of ecosystem productivity and model evaluations.

2.5 Observed and simulated vegetation O_3 sensitivity derived from dose-response relationships

To ensure a consistent intercomparison of vegetation responses across different ozone damage parameterizations, we estimate PFT-specific ozone sensitivities from the dose-response relationships (DRR) derived from each simulation. The DRR of GPP can be expressed as:

$$RGPP = b \times POD_y + c$$

where RGPP denotes the relative change in GPP under O_3 exposure compared with the O3OFF experiment, and the ozone dose is characterized by the annual cumulative stomatal ozone uptake (i.e., POD_y). Ozone sensitivity is quantified as the slope of the linear relationship between RGPP and POD_y, which is then used in comparisons between different PFTs and schemes. Observations of ozone sensitivity are assembled from recent literatures to evaluate the performance of the simulated dose-response relationships. We obtain the observational results from by Ma et al. (2023) and Li et al. (2024), who compiled field measurements and O_3 fumigation experiments across a range of literature sources. For Ma et al. (2023), PFT-specific O_3 sensitivities were compiled from published studies based on regressions between biotic indicators and POD_y. We use the median value for each PFT as the observed sensitivity and the reported minimum-maximum range as an uncertainty interval. In contrast, Li et al. (2024) provided a comprehensive database of >4000 paired observations of photosynthesis and POD_y. We therefore derive the slopes of PFT-specific dose-response relationships directly from the raw data as the observed ozone sensitivity (Fig. S3). Uncertainty was quantified using bootstrap resampling (1000 iterations), with the 2.5^{th} and 97.5^{th} percentiles of the slope distribution taken as the confidence interval.

https://doi.org/10.5194/egusphere-2026-1335
Preprint. Discussion started: 18 March 2026

3 Results

3.1 Implementation of O_3-vegetation damage schemes and site-level evaluation

Six ozone-vegetation damage parameterizations were implemented in SSiB4/TRIFFID against field observations at two flux-tower sites with O_3 flux measurements. Both sites have been widely used in previous studies to investigate ozone-vegetation interactions and dry deposition (Ducker et al., 2018; Li et al., 2020; Lin et al., 2020). Figure 1 shows the simulated O_3 flux and GPP for US-Ha1 in 1998 and FI-Hyy in 2009, while the other two site-years (US-Ha1, 1999; FI-Hyy, 2008) are shown in the supplementary materials (Fig. S4). Overall, all schemes agree well with observations in both amplitude and seasonality of stomatal O_3 flux and GPP. However, stomatal O_3 flux tends to be underestimated in November-February, likely due to the simulated weak photosynthetic activity in winter (Fig. 1).

Among the five schemes, L2015 and L2024 generally exhibit smaller biases in simulated O_3 flux, followed by LMApft and CS2007. The S2007 scheme consistently simulates the lowest ozone uptake (Fig 1b and e). All schemes indicate O_3-induced reductions in GPP at both sites, while the simulated magnitude varies substantially across parameterizations. At US-Ha1, L2015 produces the weakest ozone-induced GPP reduction, followed by CS2007 and LMApft, whereas L2024 and S2007 yield the largest reductions (Fig. 1c). At FI-Hyy, the simulated O_3 impacts on GPP is weaker with a smaller inter-scheme spread. The CS2007 and LMApft simulate relatively smaller reductions, whereas L2015, L2024, and S2007 produce larger GPP losses (Fig. 1e). We further quantified inter-scheme differences by computing the mean absolute error (MAE) of simulated stomatal O_3 flux and GPP relative to site observations (Fig. S5). For stomatal O_3 flux, L2024 consistently yields the lowest MAE across all four site-years. For GPP, however, the MAE varies across site-years: L2015 shows the smallest MAE at FI-Hyy, while L2024 and CS2007 produce the lowest errors in US-Ha1. Although the magnitude of simulated GPP response differs among the schemes, accounting for O_3 effects consistently reduces GPP bias relative to the O3OFF experiment. Overall, all schemes reproduce the observed magnitude and seasonal cycle of both stomatal O_3 flux and GPP values. Among the schemes, L2024 shows the best agreement with observations for stomatal O_3 flux, as indicated by the lowest MAE across sites.

3.2 Estimation of O_3-induced vegetation damage in China in the 2010s

In regional simulation experiments, we first quantified the baseline performance of SSiB4/TRIFFID over China under the control experiment without O_3-induced vegetation damage (i.e. O3OFF). Simulated GPP and LAI are compared with satellite measurements, including GPP from GOSIF and LAI from GLASS. The results indicate that SSiB4/TRIFFID is capable of realistically reproducing vegetation growth and photosynthetic activity over China, with high spatial correlations of 0.94 for GPP and 0.89 for LAI in the growing season (April–September), respectively (Fig. 2 and S6). Consistent with satellite observations, high GPP values are found in southern China and eastern China. At the national scale, the O3OFF experiment generally overestimates GPP and LAI compared to observations, with a positive bias of 14.88% in GPP and 22.78% in LAI, respectively.

https://doi.org/10.5194/egusphere-2026-1335
Preprint. Discussion started: 18 March 2026

Using hourly surface ozone concentrations from HrSOD, we quantified O_3-induced vegetation damage over China with the six ozone–vegetation damage parameterizations implemented in SSiB4/TRIFFID model. Across all schemes, ambient ozone pollution substantially suppresses vegetation photosynthesis nationwide. The largest reductions in GPP occur in southern China, where densely-distributed vegetation coincides with elevated ozone exposure. In eastern China, despite the comparatively lower vegetation distribution, severe ozone pollution still leads to pronounced photosynthetic damage. Based on the multi-scheme assessment, we estimate an average O_3-induced GPP loss over China by 20.77%, with a spread of 15.61–31.01% among the six schemes. As a result, the national annual GPP decreases from 8.93 PgC in O3OFF to 7.07 PgC, with an inter-scheme range of 6.16-7.53PgC. The seasonal evolution of ozone-induced GPP loss exhibits a clear unimodal pattern, with the largest reductions occurring during summer, coincident with peak ozone concentrations and maximum vegetation growth.

Overall, ambient ozone pollution leads to substantial reductions in GPP across China. Comparisons against observations further indicate that implementation of O_3 damage schemes into land surface model can improve the simulation of carbon fluxes over China. Meanwhile, the six parameterizations yield marked discrepancies in O_3-induced GPP damage, as evidenced by the large inter-scheme spread as shown by the shading in Fig. 3c. These divergences are particularly pronounced during the late growing season. At the annual scale, the inter-scheme spread is comparable in magnitude to the GPP loss itself, which indicates a large uncertainty in assessing O_3-induced GPP reductions in China. Given the severe ozone burden in China and the pronounced differences among current parameterizations, a comprehensive investigation is needed to diagnose inter-scheme divergences and to evaluate their performance in China, which is crucial for narrowing the uncertainties in simulated O_3 impacts on vegetation and improving regional GPP simulations over China.

3.3 Inter-scheme variability in PFT-specific ozone sensitivity

Figure 4 shows the spatial distribution of O_3-induced GPP loss simulated by the six ozone–vegetation damage parameterizations. All schemes reproduce a similar spatial pattern, with the strongest losses in southern China, followed by eastern China, and weak O_3 impacts are found in northwestern China where vegetation is sparsely distributed and baseline GPP is low. In contrast to the consistent spatial pattern, the simulated GPP loss differs substantially among the six schemes: L2024 and S2007 yield the strongest O_3-induced GPP reductions, while L2015 and CS2007 simulate the weakest responses, and the LMA-based schemes (LMAgrid and LMApft) show intermediate reductions. The O_3-induced suppression in photosynthesis reduces carbon assimilation of plants, which in turn constraints vegetation growth and results in a modest decrease in LAI (Fig. S7). The schemes also diverge in simulated stomatal O_3 uptake and associated impacts on stomatal conductance, with L2015 and L2024 yielding the highest ozone uptake and S2007 the lowest, which consists with the site-level evaluation.

However, although higher O_3 flux generally correlates with increased photosynthetic and stomatal damage within a single scheme, this relationship is not consistent across different parameterizations (Fig. 4, S8 and S9). For example, S2007 yields significant reductions in photosynthesis and stomatal conductance despite a relatively low stomatal O_3 uptake. In contrast, both

https://doi.org/10.5194/egusphere-2026-1335
Preprint. Discussion started: 18 March 2026

CS2007 and LMA-based schemes show weaker O_3-induced vegetation damage despite moderate O_3 uptake. L2015 and L2024 exhibit strong stomatal O_3 uptake, but the photosynthetic response of L2015 is markedly weaker than that of L2024. These variations suggest considerable differences in vegetation sensitivity to O_3 across the schemes and highlight the need for comprehensive assessment of O_3 sensitivity simulated by each parameterization. In the subsequent analysis, we examine the vegetation-ozone sensitivity of the six schemes and assess their performances against observation constraints.

Base on the simulated ozone-induced vegetation damage over China, we derive the response relationships between GPP and O_3 uptake for each of the six parameterizations. Specifically, we evaluate the relative change in GPP (RGPP) as a function of POD_y at the annual scale. As shown in Fig. 5, significant discrepancies arise among the schemes in the representation of RGPP-POD_y relationship. Under the L2015 scheme, RGPP exhibits little sensitivity to increasing O_3 uptake. This is because the O_3 damage factor in L2015 remains constant for many PFTs, lacking a response to additional O_3 absorption. As a result, while O_3-induced GPP damage is simulated, the RGPP response to POD_y is not captured. In contrast, S2007 displays the highest ozone sensitivity, which explains the substantial reductions in GPP under lower stomatal O_3 uptake. The remaining schemes demonstrate moderate sensitivities with a small inter-scheme discrepancy: L2024 show a higher sensitivity than the LMA-based schemes, and the O_3 sensitivity of CS2007 is slightly lower.

In addition to inter-scheme differences, significant variation in ozone sensitivity is observed across PFTs. According to our results, C3 vegetation, shrubs, and deciduous broadleaf forests (DBF) exhibit relatively high ozone sensitivity, whereas evergreen broadleaf forests (EBF), evergreen needleleaf forests (ENF), and C4 vegetation show greater tolerance to ozone exposure (Fig. 5). To quantify vegetation ozone sensitivity at the PFT level, we used the slope of the RGPP–POD_y relationships in Fig. 5 as an indicator of ozone sensitivity for each PFT. These modelled sensitivities were then compared against observations from Ma et al. (2023) and Li et al. (2024), who synthesized field measurements and experimental results from peer-reviewed literatures. The detailed methodology used to derive ozone sensitivity from simulation and observation is provided in Sect. 2.

Figure 6 compares the modelled PFT-specific O_3 sensitivities with observation datasets from Ma et al. (2023) and Li et al. (2024). Given the differences in observed O_3 sensitivity between these two sources, we present the results from both datasets. Parameterizations exhibiting O_3 sensitivities within the confidence intervals of both datasets or between them are considered the most reliable. Schemes that fall within the confidence interval of only one dataset are considered moderately reliable, while those deviate from both ranges are regarded less reliable. For EBF, the L2024, CS2007, and the LMA-based schemes fall within the confidence interval of Ma et al. (2023) and exhibit sensitivities between the two observational datasets. L2015 substantially underestimates O_3 sensitivity. As for S2007, a positive slope has been fitted to the RGPP–POD_y relationship, which is inconsistent with expected behaviour and likely caused by sparse sampling and its distribution. For ENF, L2024, S2007, and LMAgrid agree well with the two observational estimates, while L2015, CS2007, and LMApft fall outside the uncertainty range. For C3 and C4 grasses, sensitivity estimates remain highly uncertain due to the limited availability of observational data. For C3 grasses, L2024 and the LMA-based schemes agree well with Ma et al. (2023), whereas for C4 vegetation, S2007 exhibits the closest agreement with both observational datasets. For shrubs, L2024, CS2007, and the LMA-

https://doi.org/10.5194/egusphere-2026-1335
Preprint. Discussion started: 18 March 2026

based schemes remain consistent with observations. For DBF, the LMA-based schemes show the strongest consistency, while L2024, S2007, and CS2007 also fall within the observational confidence intervals.

Finally, we averaged the observational ozone sensitivities from the two datasets and benchmarked the simulated sensitivities across PFTs. Scheme performance was assessed using the MAE between modeled and observed sensitivities. Figure 7 shows that L2024 matches observations most closely (mean bias = 0.219; MAE = 0.274), followed by LMAgrid and LMApft with similar average biases. CS2007 consistently underestimates ozone sensitivity across all PFTs. S2007 exhibits significant PFT-dependent errors, which results in a large MAE despite a modest mean bias. L2015 shows very weak ozone sensitivity, implying that vegetation responses to additional ozone uptake are not realistically represented. Overall, our assessment base on vegetation O_3 sensitivity offers a clear, observation-based benchmark for evaluating reliability of O_3-vegetation damage parameterization schemes. Among the six schemes, L2024 shows the most consistent agreement with observed sensitivities across PFTs, and the LMA-based approaches show similarly good performance with modest bias. This benchmark helps identify the sources of inter-scheme differences in simulated ozone damage and provides a consistent basis for scheme comparison that is less affected by model-dependent biases in simulated GPP.

3.4 Trait-based refinement of cumulative uptake of O_3

Although the L2024 scheme performs well in the inter-scheme comparison, it shows a limitation in representing seasonal dynamics of vegetation physiology. Unlike S2007 and the LMA-based schemes, which diagnose O_3 damage from instantaneous stomatal O_3 flux, L2024 links the O_3 damage factor to CUO, which is updated each timestep through uptake, decay, and healing process (see Sect. 2.2). Because the decay term is implemented only for evergreen species, CUO accumulates strongly for other PFTs, leading to a persistent increasing suppression of photosynthesis over the growing season (Fig. 8a). Consequently, this carry-over effect from early-season CUO accumulation leads to a pronounced late-season GPP reduction and biases the simulated seasonal cycle (Fig. 8c).

To address these issues, we implement two adjustments to L2024. First, we extend the decay term of CUO to all PFTs, instead of restricting it to evergreen species. Second, we updated the key parameter l_{leaf} by prescribing PFT-specific values using observed leaf lifespan estimates. These updates aim to prevent the unrealistic CUO accumulation and to reduce the overestimation of O_3 vegetation damage towards the late growing season. As shown in Fig. 8a, the revised formulation ($L2024_{modify}$) shows a pronounced reduction in CUO accumulation with a similar instantaneous stomatal O_3 uptake, indicating a revised CUO dynamics rather than changes in stomatal absorption. The reduced CUO weakens O_3-induced GPP damage, lowering the annual GPP bias by 25.8% and increasing the spatial correlation with observations (Fig. 8b). Notably, the improvement is stronger under high-GPP conditions, where the original L2024 scheme exhibits pronounced underestimations, implying that the overestimation of GPP damage is largely reduced in high vegetated regions and seasons. As for seasonality, the reduced CUO limits the carry-over of accumulated O_3 stress. Consequently, GPP increases later in the growing season, particularly in summer and autumn with high O_3 exposures and high ecosystem productivity, which improves the simulated seasonal cycle of GPP compared with observations (Fig. 8c). Spatially, the strongest GPP recovery occurs over southern China

https://doi.org/10.5194/egusphere-2026-1335
Preprint. Discussion started: 18 March 2026

(Fig. 8d), a hotspot of stomatal O_3 uptake and O_3-induced GPP reductions (Fig. 8d). Overall, introducing the trait-based decay formulation markedly reduces the carry-over of O_3 stress in the original L2024 scheme and improves the simulated magnitude and seasonality of GPP, with the largest corrections concentrated in densely vegetated areas of southern China.

4. Discussions

4.1 PFT-specific O_3 sensitivity in current O_3 vegetation damage parameterizations

In this study, we implemented six up-to-date O_3 vegetation damage parameterizations into SSiB4/TRIFFID to assess the impact of surface ozone pollution on vegetation in China. Our analysis revealed significant variation in the simulated ozone sensitivity across these schemes, largely attributed to discrepancies in how vegetation–ozone sensitivity is represented within each scheme.

Despite the diverse physical processes emphasized by the individual schemes, all flux-based ozone damage parameterizations consistently recognize that vegetation ozone sensitivity varies substantially across plant functional types (PFTs). This variability is influenced by multiple factors, including foliar structural traits, stomatal regulation, antioxidant capacity, detoxification pathways, and underlying differences in photosynthetic metabolism, such as C3 versus C4 pathways (Hayes et al., 2007; Li et al., 2017; Agathokleous et al., 2020). Empirical studies have shown that evergreen species generally exhibit greater resilience to ozone-induced oxidative stress compared to deciduous species, likely due to higher antioxidant enzyme activities and larger leaf mass per area (LMA) in evergreen leaves (Li et al., 2017). Leaves with high LMA are typically characterized by thicker or denser palisade mesophyll layers, which reduce ozone exposure per unit leaf mass and enhance antioxidant capacity through a larger apoplastic compartment (Feng et al., 2018). Therefore, LMA has been identified as a key factor in governing ozone sensitivity at the leaf level in recent studies (Agathokleous et al., 2020; Ma et al., 2023; Feng et al., 2021). In addition, species with shorter leaf lifespans tend to exhibit higher ozone sensitivity. Fast-growing species, such as grasses and crops, typically have lower leaf toughness and higher specific leaf area, which results in weaker structural and biochemical defences against environmental stressors, including ozone exposure (Ma et al., 2023). Moreover, recent studies have observed greater ozone sensitivity in C3 compared to C4 plants (Li et al., 2023). This difference can be attributed to the CO2-concentrating mechanism in C4 plants, which improves photosynthetic efficiency while reducing stomatal conductance. The lower stomatal conductance in C4 plants limits ozone uptake, while the higher photosynthetic efficiency supports enhanced detoxification processes and antioxidant biosynthesis, thereby reducing ozone-induced damage and increasing ozone tolerance.

Consistent with these findings, our results indicate that shrubs, C3 grasses, and deciduous broadleaf trees exhibit higher ozone sensitivity, whereas C4 grasses, evergreen broadleaf forests, and evergreen needleleaf forests tend to be less sensitive (Fig. 6). Notably, the insufficient observation evidence of C3 and C4 species limited the ability to accurately assess ozone sensitivity between schemes, resulting in a broad confidence interval (CIs) when comparing simulations with observed data. By comparing the results of all the schemes, we found that the recently-developed L2024 scheme shows the closest agreement

https://doi.org/10.5194/egusphere-2026-1335
Preprint. Discussion started: 18 March 2026

with observations in terms of simulated ozone sensitivity. This advantage can be attributed to its nonlinear formulation of plant responses to CUO, which is built upon an extensive database of more than 4,000 experimental measurements (Li et al., 2024). Similarly, the LMA-based approaches also produced relatively accurate ozone sensitivity estimates due to its uniformed expression based on PFT- or grid-specific LMA, a key trait that governs ozone sensitivity across diverse plant species and functional types (Agathokleous et al., 2020; Feng et al., 2018). In contrast, S2007 and L2015 schemes exhibited notable limitations in representing plant ozone sensitivity. These shortcomings primarily reflect the scarcity of observational and experimental data used to develop and constrain these parameterizations (Li et al., 2024). Consequently, these earlier schemes are less reliable in simulating ozone sensitivity compared to the more recent L2024 and LMA-based parameterizations.

In summary, our study applies a sensitivity-based comparison approach that offers a reliable and robust framework for cross-scheme evaluation. This approach avoids the influence of model-specific biases and mitigates potential disturbance caused by model configurations. Our results underscore the importance of incorporating both observational constraints and mechanistic understanding from field experiments into O_3 sensitivity parameterizations. This is essential for improving the realism of O_3-damage simulations and for developing more robust parameterizations that can represent the diverse responses of terrestrial ecosystems to O_3 exposure.

4.2 Improved CUO representation with trait-informed decay and LAI-based healing

According to our evaluation, L2024 scheme captures the O_3 sensitivity most accurately, benefiting from a nonlinear response formulation constrained by extensive O_3 fumigation experiments. However, because the CUO-based formulation allows O_3 stress to accumulate through the growing season without a sufficient decay process for most PFTs, it can induce a strong O_3 damage to plants during the mid-to-late growing season. To fix this over-accumulation, we extend the decay term to all PFTs, rather than restricting it to evergreen species in the original version. This modification substantially reduces CUO from July to November, thereby alleviating the O_3-induce damage in late growing season and improving the spatiotemporal patterns of simulated GPP.

Experimental and modelling studies consistently suggest that indicates that vegetation responses to ozone exposure are often nonlinear under chronic exposure, implying a diminishing marginal impact of increasing POD_y as defence and tolerance mechanisms are activated (Heath et al., 2009; Li et al., 2024). This nonlinearity likely reflects two complementary pathways: avoidance, through stomatal regulation, and confrontation, through antioxidation, detoxification and repair processes (Sharma et al., 2012; Scimone et al., 2024). On the one hand, exposure to O_3 can severely impair photosynthesis and stomatal functions, with the resulting stomatal closure acting as negative feedback that constraints further O_3 uptake (Li et al., 2017). On the other hand, elevated O_3 exposure alters hormone regulation and increases apoplastic antioxidants capacity (e.g., ascorbate, phenolic, glutathione), which can directly react with O_3 and scavenge ROS, thereby enhancing the O_3 tolerance (Castagna and Ranieri, 2009; Heath et al., 2009; Li et al., 2023). O_3 is also known to damage leaf cells and accelerate senescence, but plants may offset these effects through cellular repair and the production of new leaves (Heath and Taylor, 1997; Grulke and Heath, 2020). Taken together, these mechanisms indicate that O_3 damage is moderated over time, and the physiological-related detoxification

https://doi.org/10.5194/egusphere-2026-1335
Preprint. Discussion started: 18 March 2026

process cannot be represented by a fixed POD_y threshold (Heath et al., 2009). Motivated by this evidence, we apply the decay term for all PFTs to represent the physiological removal of O_3-induced oxidative stress (detoxification), accompanied by the healing term to account for the emergence of new, undamaged leaves (Felzer et al., 2009; Li et al., 2024). With these modifications, CUO accumulation is markedly reduced through the growing season, and GPP simulations improve in both spatial patterns and seasonal cycles. This trait-based decay refinement acknowledges that O_3 impacts on vegetation are dynamically regulated by physiological process and feedbacks, rather than solely controlled by the rise in O_3 uptake.

4.3 Limitations

In this study, we integrated six flux-based ozone–vegetation damage parameterizations into SSiB4/TRIFFID, and quantified the impacts of tropospheric ozone on terrestrial vegetation in China in the 2010s. Based on comprehensive evaluation of inter-scheme differences and refinement of ozone decay representations, our work provides a more comprehensive assessment of O_3-induced GPP losses in China. Nevertheless, there are some limitations that should be acknowledged.

First, nitrogen deposition was not considered in this study. Given that nitrogen fertilization can alleviate nutrient limitation and thereby partially offset ozone-induced productivity losses (Ren et al., 2011), this exclusion therefore introduces uncertainty into the estimated ozone damage, especially for nitrogen-limited regions. Moreover, although the effects of CO_2 and vapor pressure deficit (VPD) on vegetation were included in our simulations, their interactions with ozone damage were not explicitly separated. Both elevated CO_2 and increased VPD can regulate stomatal conductance and thereby modify stomatal O_3 uptake. Therefore, the simulated ozone responses may incorporate indirect effects of these concurrent drivers, introducing additional uncertainty in the attribution of O_3 impacts. In addition, our offline framework is not able to capture feedbacks mediated by land-atmosphere coupling. Previous studies indicate a positive ozone–vegetation feedback, whereby O_3-induced physiological and biophysical responses can both reduce O_3 removal and enhance photochemical production. In particular, O_3-driven stomatal closure weakens canopy O_3 uptake and deposition, while the associated surface warming accelerates biogenic VOC emissions and ozone formation (Jin et al., 2023; Cao et al., 2024). Accordingly, the absence of land-atmosphere-chemistry feedbacks in our offline framework may contribute to a slightly weaker response and a modest underestimation of O_3-induced vegetation damage relative to coupled simulations (Zhu et al., 2022; Jin et al., 2023). Our results should therefore be interpreted as conservative with respect to fully coupled modelling, and our intercomparison and refinement efforts offers a solid baseline for quantifying ozone-vegetation interactions under coupled frameworks.

5. Conclusions

China is widely recognized as a hotspot of ozone pollution and associated vegetation impacts. As surface O_3 persist rise while observations on O_3-vegetation interactions remain limited, quantitative assessments increasingly rely on numerical models and the parameterizations. By implementing six flux-based schemes in a unified SSiB4/TRIFFID framework, we estimate that O_3 reduced China's national GPP by nearly 20% in the 2010s, yet losses vary markedly across schemes (15%–

https://doi.org/10.5194/egusphere-2026-1335
Preprint. Discussion started: 18 March 2026

31%). The inter-scheme discrepancies arise from the representation of plant O_3 sensitivity and its dependence on PFT. Comparisons with published dose–response relationships indicate that the recently developed L2024 and LMA-based schemes better reproduce observed O_3 sensitivities, consistent with their incorporation of broad observational evidence and trait-informed physiological constraints. Furthermore, we refined the L2024 formulation by extending the decay process to all PFTs and updating the leaf longevity parameter with observations. The revised formulation reduces the unrealistic accumulation of O_3 stress during the growing season and improves the simulated spatial distribution and seasonal cycle of GPP. Overall, our work highlights the importance of observation- and physiology-based constraints on ozone damage parameterizations for robust assessment of O_3 impacts on vegetation. Looking ahead, expanding flux measurements and fumigation experiments, particularly in China's natural ecosystems, will tighten model constraints and improve simulation of ozone-vegetation interactions. By narrowing uncertainty, the advanced parameterizations and models can provide a firm scientific basis for policy-relevant quantification and projection of O_3-driven ecological risks and the mitigation potential of emission controls in a warming future.

https://doi.org/10.5194/egusphere-2026-1335
Preprint. Discussion started: 18 March 2026

Code availability. The codes of the SSiB4/TRIFFID model with six O_3-damage parameterizations are shared at https://doi.org/10.5281/zenodo.18927710 (Li, 2026).

Data availability. Results of all simulations (listed in Table 1 and 2) are shared at https://doi.org/10.5281/zenodo.18927710 (Li, 2026). The whole original source data are publicly available with details listed in Table S3.

Author contributions. LL, BQ, and WG designed the research, LL and SZ developed the model code, LL performed modelling, data analyses, visualization and wrote the manuscript draft. BQ, XM, CC, JC and YN helped with data collection, advised on concepts and methods, and contributed to the interpretation of the results. XH, HC, and WG reviewed and edited the paper. All authors commented on and revised the manuscript.

Competing interests. The authors declare no competing interest.

Disclaimer. Publisher's note: Copernicus Publications remains neutral with regard to jurisdictional claims made in the text, published maps, institutional affiliations, or any other geographical representation in this paper. While Copernicus Publications makes every effort to include appropriate place names, the final responsibility lies with the authors. Views expressed in the text are those of the authors and do not necessarily reflect the views of the publisher.

Acknowledgements. We acknowledge the financial support provided by our funding sources. We thank the dataset providers for sharing the data. We also thank the editors and reviewers for their valuable feedback on the revisions.

Financial support. This study is supported by the National Natural Science Foundation of China (grant nos. 424B2041, 42175136 ,42305033), and the Jiangsu Collaborative Innovation Center for Climate Change.

https://doi.org/10.5194/egusphere-2026-1335
Preprint. Discussion started: 18 March 2026

Figures

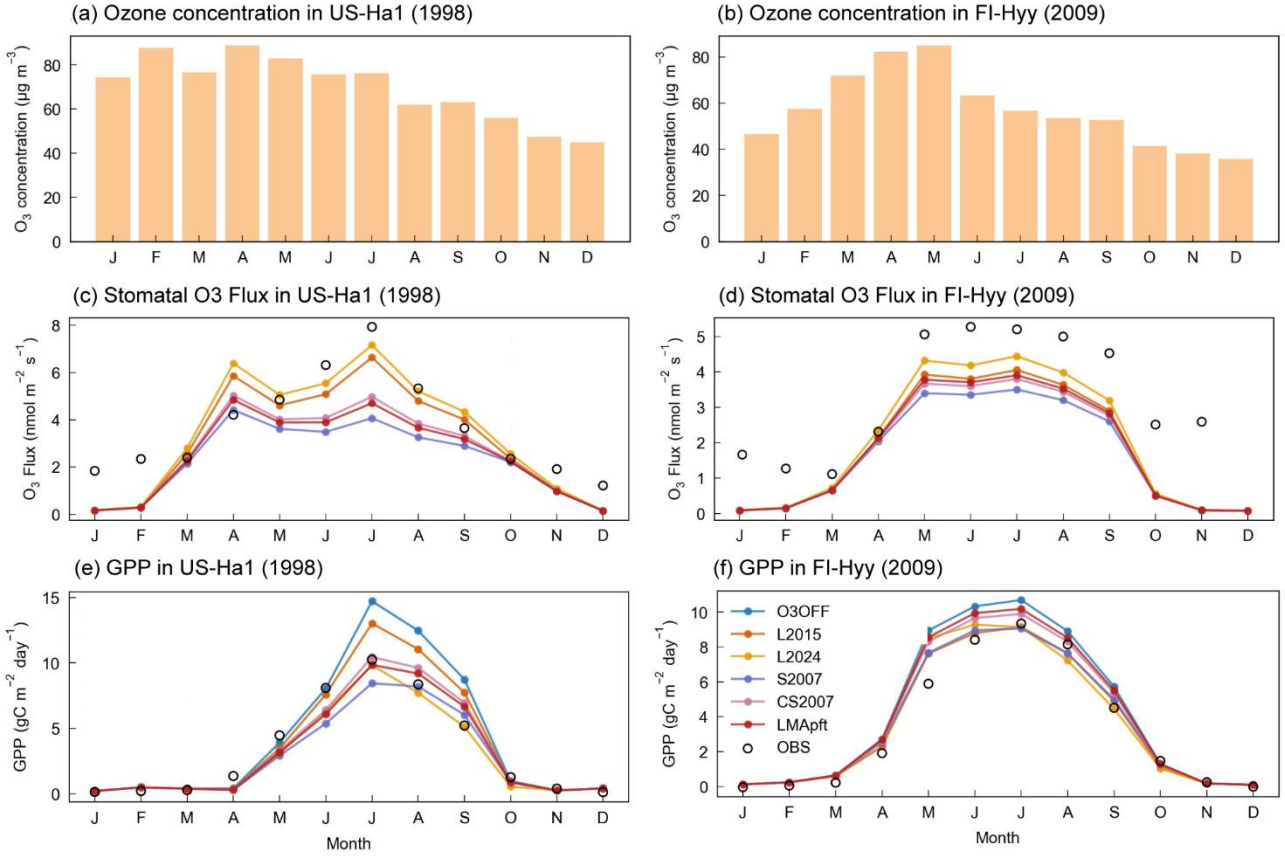

Figure 1. Site-level observations and simulations of monthly ozone concentration **(a, b)**, stomatal ozone flux **(c, d)**, and GPP **(e, f)** for US-Ha1 (1998) and FI-Hyy (2009), respectively. Colored lines denote different ozone damage parameterizations, bars and symbols indicate field observations.

https://doi.org/10.5194/egusphere-2026-1335
Preprint. Discussion started: 18 March 2026

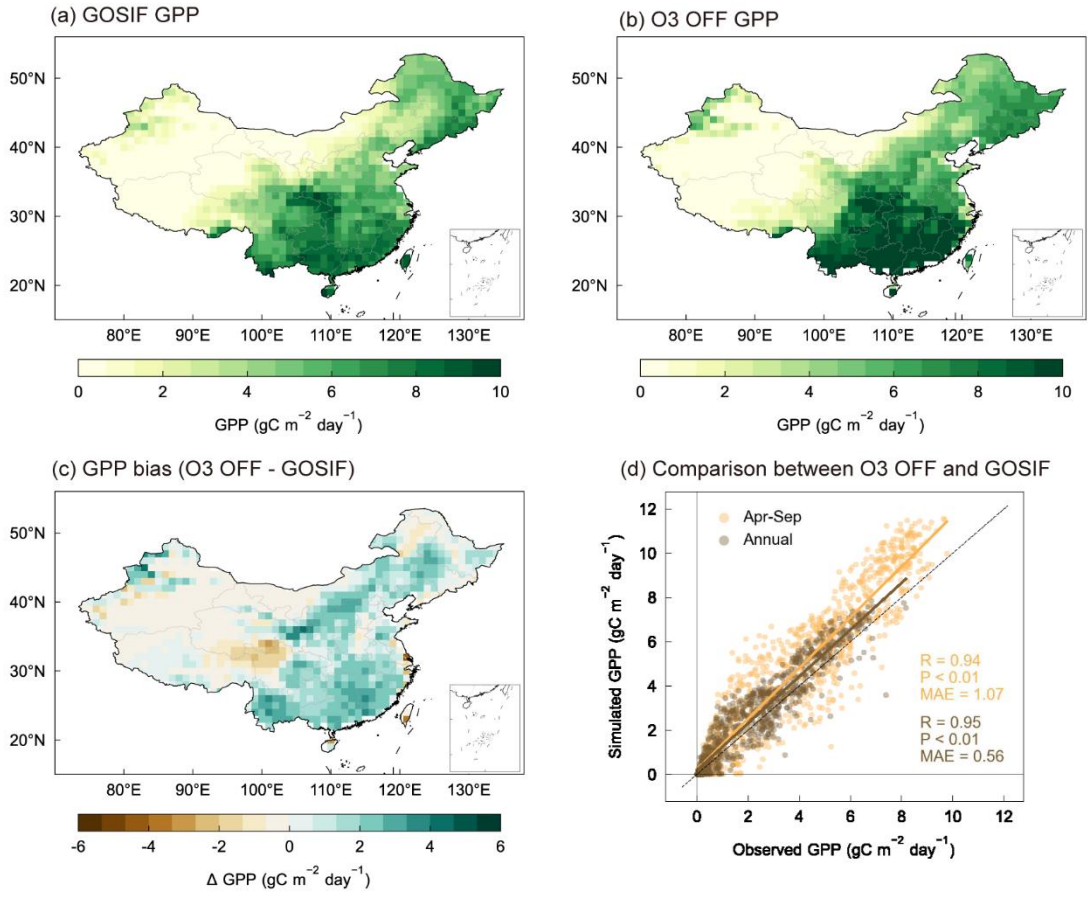

Figure 2. Evaluation of simulated GPP against satellite-based observations over China. Panel **(a)** and **(b)** are the spatial patterns of GPP derived from GOSIF observations and O3OFF experiment, respectively. The difference between O3OFF simulation and GOSIF observation is shown in **(c)**; and **(d)** presents grid-level comparisons for growing-season (April–September) and annual GPP.

https://doi.org/10.5194/egusphere-2026-1335
Preprint. Discussion started: 18 March 2026

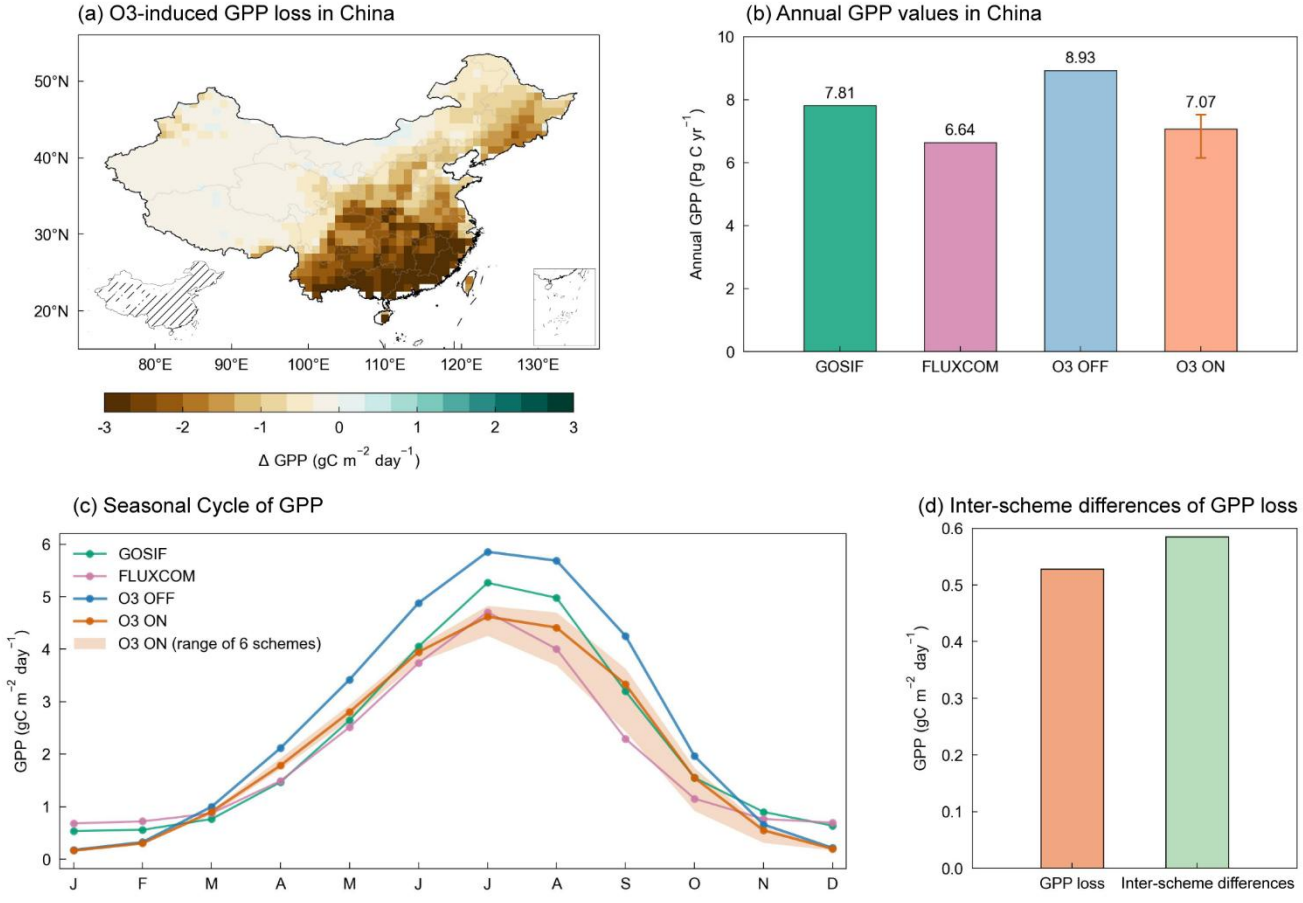

535 **Figure 3.** Simulated O_3-induced vegetation damage and the inter-scheme differences in China. **(a)** Spatial distribution of O_3-induced GPP loss averaged from all six parameterizations during the growing season (April-September). **(b)** National annual GPP from GOSIF and FLUXCOM benchmarks compared with simulations under O3 OFF and O3 ON conditions. The O3 ON shows the average from six experiments, with the error bar indicating inter-scheme discrepancies. **(c)** Seasonal cycle of GPP in China, with shading indicating the range across the six O_3 damage schemes. **(d)** Comparison between averaged GPP
540 loss and inter-scheme differences of the simulations.

https://doi.org/10.5194/egusphere-2026-1335
Preprint. Discussion started: 18 March 2026

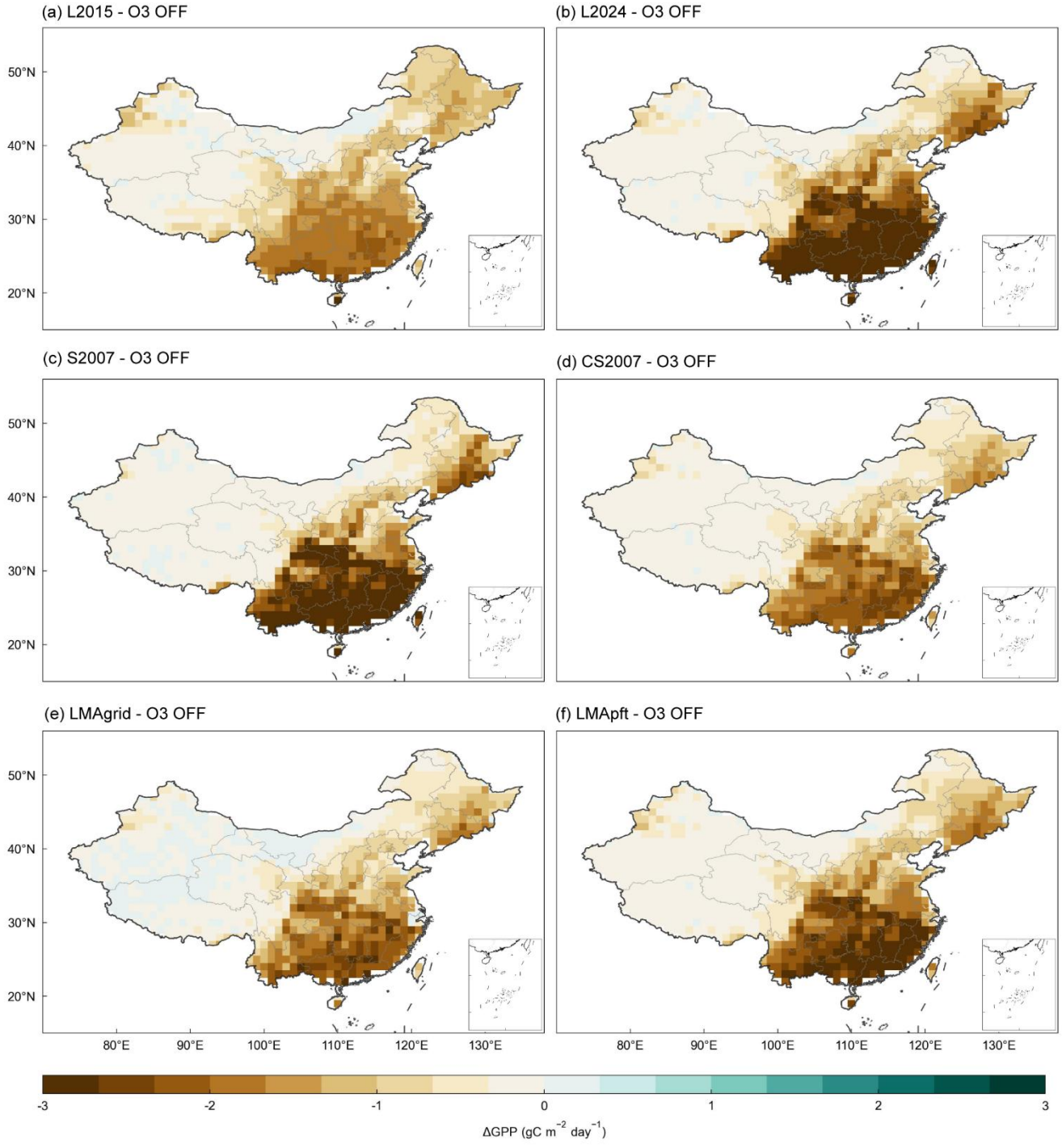

Figure 4. Comparison of ozone-induced GPP loss in China simulated by six damage parameterizations. The panels show the simulated O_3 damage during the growing season (from April to September) for **(a)** L2015, **(b)** L2024, **(c)** S2007, **(d)**

https://doi.org/10.5194/egusphere-2026-1335
Preprint. Discussion started: 18 March 2026

CS2007, **(e)** LMAgrid, and **(f)** LMApft, respectively.

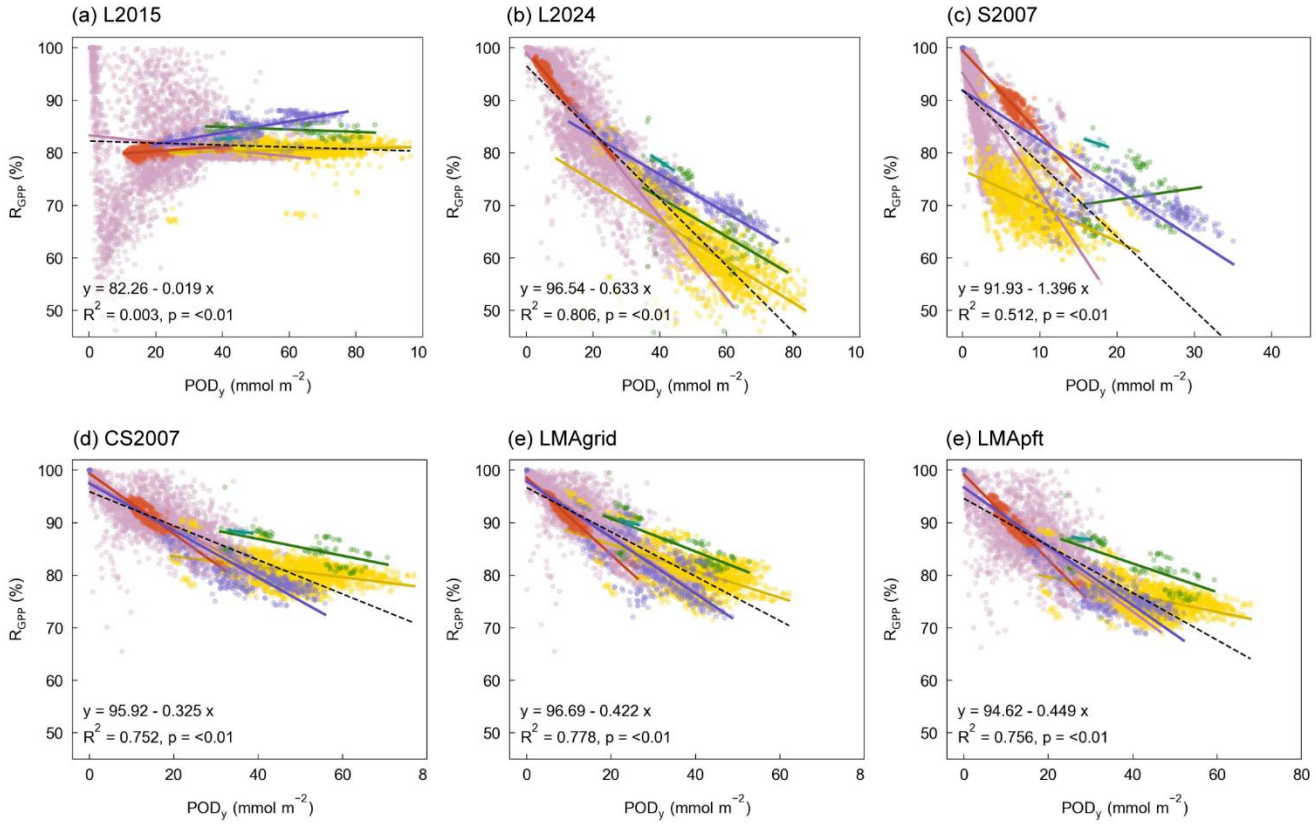

Figure 5. Dose-response relationships between relative gross primary productivity (RGPP) and POD_y for six ozone damage parameterizations: **(a)** L2015, **(b)** L2024, **(c)** S2007, **(d)** CS2007, **(e)** LMAgrid, and **(f)** LMApft. Each point represents grid-level values, with colors denoting different plant functional types. Solid lines show PFT-specific linear fits for each scheme, and the dashed lines indicate the overall dose–response relationship for each parameterization across all PFTs. Regression equations and coefficients of determination for each scheme are reported in the corresponding panel.

https://doi.org/10.5194/egusphere-2026-1335
Preprint. Discussion started: 18 March 2026

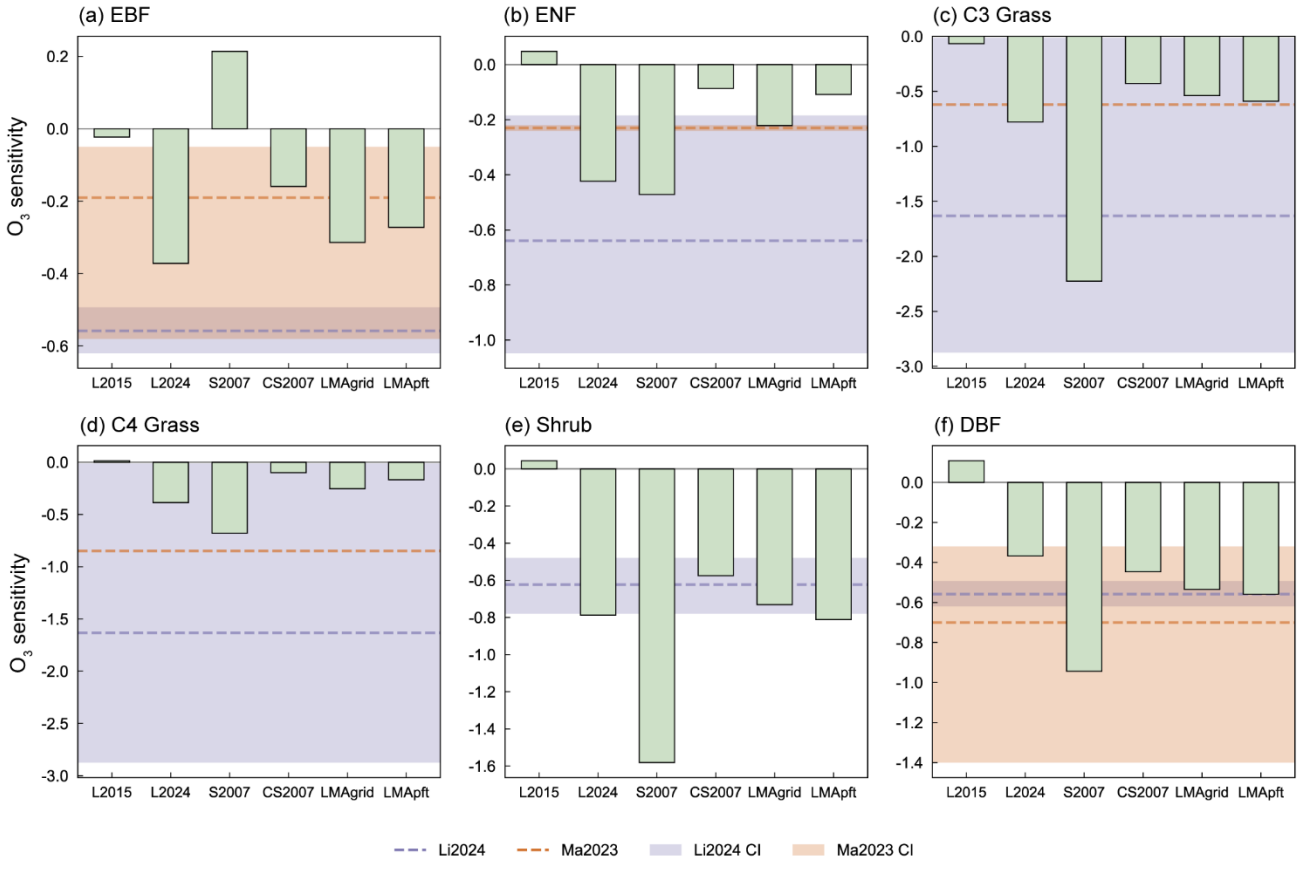

Figure 6. PFT–specific ozone sensitivity derived from the dose-response relationships for six ozone damage parameterizations. Results are shown for **(a)** evergreen broadleaf forest (EBF), **(b)** evergreen needleleaf forest (ENF), **(c)** C3 grass, **(d)** C4 grass, **(e)** shrubland, and **(f)** deciduous broadleaf forest (DBF), respectively. Bars denote the simulated ozone sensitivity for each scheme, while shaded bands and dashed lines indicate observational constraints (central estimates and confidence intervals) compiled by Ma et al., (2023) and Li et al., (2024), respectively.

https://doi.org/10.5194/egusphere-2026-1335
Preprint. Discussion started: 18 March 2026

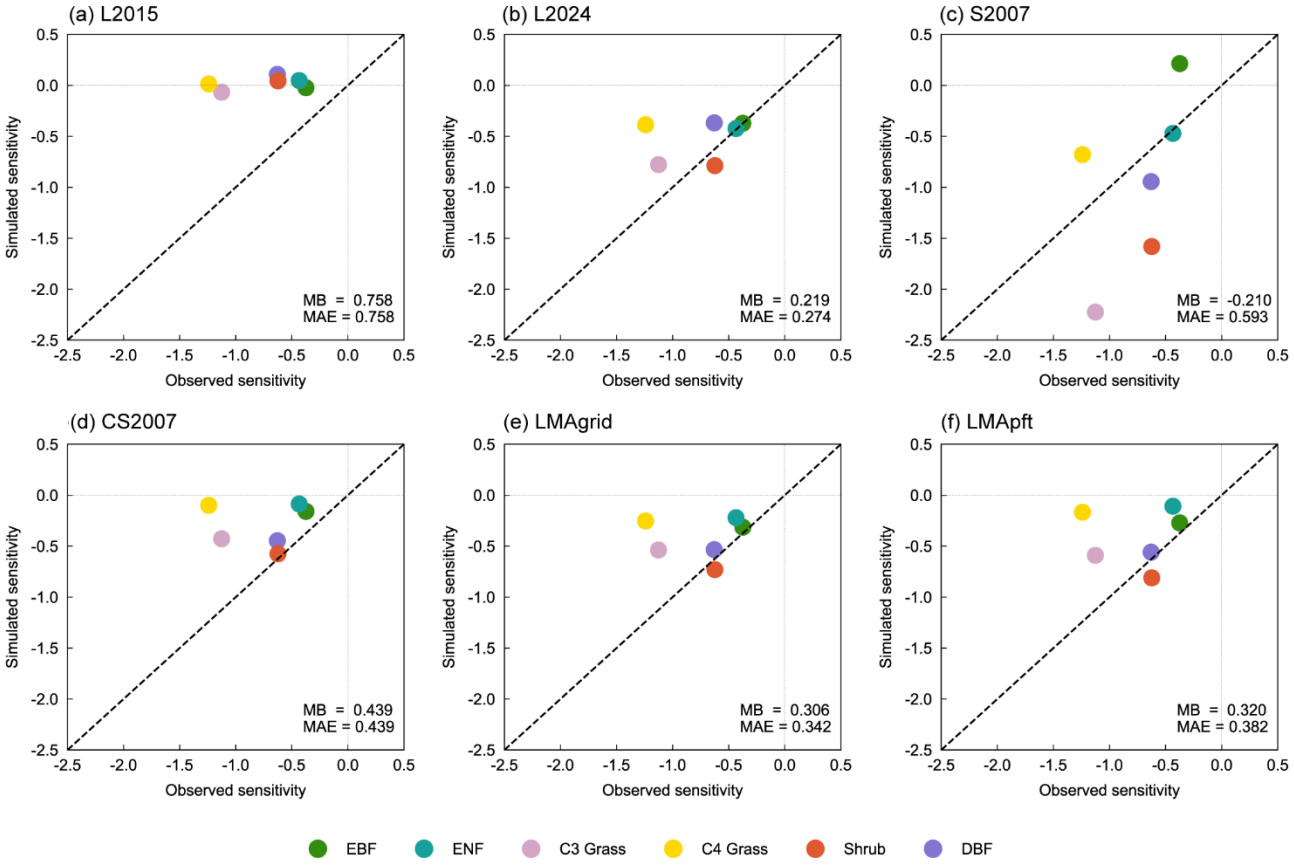

Figure 7. Comparison between simulated and observed ozone sensitivity for six ozone damage parameterizations. For each scheme, scatter plots show ozone sensitivity simulated for different plant functional types (PFTs) against corresponding observational estimates, with colors denoting each PFTs. The 1:1 line indicates agreement between simulations and observations. The mean bias (MB) and mean absolute error (MAE) of each scheme are reported in panels to summarize the deviation of simulated ozone sensitivity from observations.

https://doi.org/10.5194/egusphere-2026-1335
Preprint. Discussion started: 18 March 2026

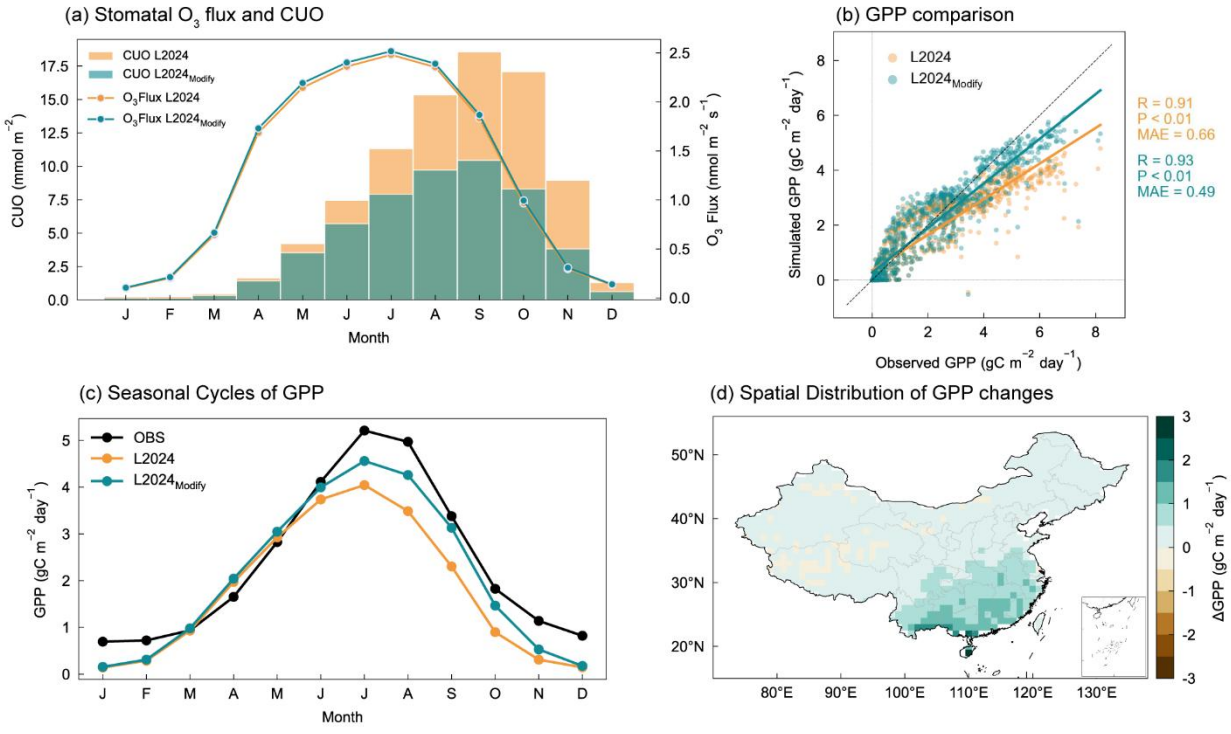

Figure 8. Comparison between the original and refined L2024 parameterizations. **(a)** Instantaneous stomatal ozone flux and cumulative uptake of ozone (CUO) simulated by the original L2024 and the refined L2024 formulation (L2024$_{modify}$). **(b)** Grid-level comparison of simulated and observed GPP for the two formulations. **(c)** Seasonal cycles of GPP from observations, the original L2024, and the refined L2024$_{modify}$ scheme. **(d)** Spatial patterns of GPP changes between the original and refined L2024 formulations.

https://doi.org/10.5194/egusphere-2026-1335
Preprint. Discussion started: 18 March 2026

References

Agathokleous, E., Feng, Z., Oksanen, E., Sicard, P., Wang, Q., Saitanis, C. J., Araminiene, V., Blande, J. D., Hayes, F., Calatayud, V., Domingos, M., Veresoglou, S. D., Penuelas, J., Wardle, D. A., De Marco, A., Li, Z., Harmens, H., Yuan, X., Vitale, M., and Paoletti, E.: Ozone affects plant, insect, and soil microbial communities: A threat to terrestrial ecosystems and biodiversity, Sci. Adv., 6, 10.1126/sciadv.abc1176, 2020.

Ainsworth, E. A., Yendrek, C. R., Sitch, S., Collins, W. J., and Emberson, L. D.: The Effects of Tropospheric Ozone on Net Primary Productivity and Implications for Climate Change, Annu. Rev. Plant Biol., 63, 637-661, 10.1146/annurev-arplant-042110-103829, 2012.

Cao, J., Yue, X., and Ma, M.: Simulation of ozone–vegetation coupling and feedback in China using multiple ozone damage schemes, Atmos. Chem. Phys., 24, 3973-3987, 10.5194/acp-24-3973-2024, 2024.

Castagna, A. and Ranieri, A.: Detoxification and repair process of ozone injury: From O3 uptake to gene expression adjustment, Environ. Pollut., 157, 1461-1469, https://doi.org/10.1016/j.envpol.2008.09.029, 2009.

Cheesman, A. W., Brown, F., Artaxo, P., Farha, M. N., Folberth, G. A., Hayes, F. J., Heinrich, V. H. A., Hill, T. C., Mercado, L. M., Oliver, R. J., O' Sullivan, M., Uddling, J., Cernusak, L. A., and Sitch, S.: Reduced productivity and carbon drawdown of tropical forests from ground-level ozone exposure, Nat. Geosci., 10.1038/s41561-024-01530-1, 2024.

Collatz, G. J., Ball, J. T., Grivet, C., and Berry, J. A.: Physiological and environmental regulation of stomatal conductance, photosynthesis and transpiration: a model that includes a laminar boundary layer, Agric. For. Meteorol., 54, 107-136, https://doi.org/10.1016/0168-1923(91)90002-8, 1991.

Ducker, J. A., Holmes, C. D., Keenan, T. F., Fares, S., Goldstein, A. H., Mammarella, I., Munger, J. W., and Schnell, J.: Synthetic ozone deposition and stomatal uptake at flux tower sites, Biogeosciences, 15, 5395-5413, 10.5194/bg-15-5395-2018, 2018.

Emberson, L.: Effects of ozone on agriculture, forests and grasslands, Philosophical Transactions of the Royal Society A: Mathematical, Physical and Engineering Sciences, 378, 10.1098/rsta.2019.0327, 2020.

Felzer, B. S., Cronin, T. W., Melillo, J. M., Kicklighter, D. W., and Schlosser, C. A.: Importance of carbon-nitrogen interactions and ozone on ecosystem hydrology during the 21st century, J. Geophys. Res.-Biogeosci., 114, 10.1029/2008jg000826, 2009.

Feng, Z., Büker, P., Pleijel, H., Emberson, L., Karlsson, P. E., and Uddling, J.: A unifying explanation for variation in ozone sensitivity among woody plants, Glob. Change Biol., 24, 78-84, https://doi.org/10.1111/gcb.13824, 2018.

Feng, Z. Z., Agathokleous, E., Yue, X., Oksanen, E., Paoletti, E., Sase, H., Gandin, A., Koike, T., Calatayud, V., Yuan, X. Y., Liu, X. J., De Marco, A., Jolivet, Y., Kontunen-Soppela, S., Hoshika, Y., Saji, H., Li, P., Li, Z., Watanabe, M., and Kobayashi, K.: Emerging challenges of ozone impacts on asian plants: actions are needed to protect ecosystem health, Ecosystem Health and Sustainability, 7, 10.1080/20964129.2021.1911602, 2021.

https://doi.org/10.5194/egusphere-2026-1335
Preprint. Discussion started: 18 March 2026

Gruenhage, L., Bender, J., Weigel, H. J., and Matyssek, R.: Critical dose indices for ozone effects on vegetation, Gefahrstoffe Reinhaltung Der Luft, 78, 173-180, 2018.

Grulke, N. E. and Heath, R. L.: Ozone effects on plants in natural ecosystems, Plant Biology, 22, 12-37, 10.1111/plb.12971, 2020.

Hayes, F., Jones, M. L. M., Mills, G., and Ashmore, M.: Meta-analysis of the relative sensitivity of semi-natural vegetation species to ozone, Environ. Pollut., 146, 754-762, https://doi.org/10.1016/j.envpol.2006.06.011, 2007.

Heath, R. L. and Taylor, G. E.: Physiological Processes and Plant Responses to Ozone Exposure, in: Forest Decline and Ozone: A Comparison of Controlled Chamber and Field Experiments, edited by: Sandermann, H., Wellburn, A. R., and Heath, R. L., Springer Berlin Heidelberg, Berlin, Heidelberg, 317-368, 10.1007/978-3-642-59233-1_10, 1997.

Heath, R. L., Lefohn, A. S., and Musselman, R. C.: Temporal processes that contribute to nonlinearity in vegetation responses to ozone exposure and dose, Atmos. Environ., 43, 2919-2928, https://doi.org/10.1016/j.atmosenv.2009.03.011, 2009.

Jin, Z., Yan, D., Zhang, Z., Li, M., Wang, T., Huang, X., Xie, M., Li, S., and Zhuang, B.: Effects of Elevated Ozone Exposure on Regional Meteorology and Air Quality in China Through Ozone-Vegetation Coupling, Journal of Geophysical Research: Atmospheres, 128, e2022JD038119, https://doi.org/10.1029/2022JD038119, 2023.

Jung, M., Schwalm, C., Migliavacca, M., Walther, S., Camps-Valls, G., Koirala, S., Anthoni, P., Besnard, S., Bodesheim, P., Carvalhais, N., Chevallier, F., Gans, F., Goll, D. S., Haverd, V., Köhler, P., Ichii, K., Jain, A. K., Liu, J. Z., Lombardozzi, D., Nabel, J. E. M. S., Nelson, J. A., O'Sullivan, M., Pallandt, M., Papale, D., Peters, W., Pongratz, J., Rödenbeck, C., Sitch, S., Tramontana, G., Walker, A., Weber, U., and Reichstein, M.: Scaling carbon fluxes from eddy covariance sites to globe: synthesis and evaluation of the FLUXCOM approach, Biogeosciences, 17, 1343-1365, 10.5194/bg-17-1343-2020, 2020.

Karlsson, P. E., Tang, L., Sundberg, J., Chen, D., Lindskog, A., and Pleijel, H.: Increasing risk for negative ozone impacts on vegetation in northern Sweden, Environ. Pollut., 150, 96-106, https://doi.org/10.1016/j.envpol.2007.06.016, 2007.

Keronen, P., Reissell, A., Rannik, Ü., Pohja, T., Siivola, E., Hiltunen, V., Hari, P., Kulmala, M., and Vesala, T.: Ozone flux measurements over a Scots pine forest using eddy covariance method: Performance evaluation and comparison with flux-profile method, Boreal Environ. Res., 8, 425-443, 2003.

Li, F., Zhou, Z., Levis, S., Sitch, S., Hayes, F., Feng, Z., Reich, P. B., Zhao, Z., and Zhou, Y.: Quantifying the role of ozone-caused damage to vegetation in the Earth system: a new parameterization scheme for photosynthetic and stomatal responses, Geosci. Model Dev., 17, 6173-6193, 10.5194/gmd-17-6173-2024, 2024.

Li, J., Wang, X., Wang, Z.-H., Wang, B., Wang, C.-Z., Deng, M.-F., and Liu, L.-L.: Effects of ozone and aerosol pollution on photosynthesis of poplar leaves, Chinese Journal of Plant Ecology, 44, 854-863, 10.17521/cjpe.2020.0022, 2020.

Li, K., Jacob, D. J., Liao, H., Qiu, Y. L., Shen, L., Zhai, S. X., Bates, K. H., Sulprizio, M. P., Song, S. J., Lu, X., Zhang, Q., Zheng, B., Zhang, Y. L., Zhang, J. Q., Lee, H. C., and Kuk, S. K.: Ozone pollution in the North China Plain spreading into the late-winter haze season, Proc. Natl. Acad. Sci. U. S. A., 118, 10.1073/pnas.2015797118, 2021.

https://doi.org/10.5194/egusphere-2026-1335
Preprint. Discussion started: 18 March 2026

Li, L.: Dataset and Code for publication titled " Integrating Ozone-vegetation Damage Schemes into SSiB4/TRIFFID: Evaluation of Six Parameterizations and Refinement of Ozone Decay Process Across Plant Functional Types", Zenodo [dataset], https://doi.org/10.5281/zenodo.18927710, 2026.

Li, P., Feng, Z., Catalayud, V., Yuan, X., Xu, Y., and Paoletti, E.: A meta-analysis on growth, physiological, and biochemical responses of woody species to ground-level ozone highlights the role of plant functional types, Plant Cell Environ., 40, 2369-2380, 10.1111/pce.13043, 2017.

Li, S., Leakey, A. D. B., Moller, C. A., Montes, C. M., Sacks, E. J., Lee, D., and Ainsworth, E. A.: Similar photosynthetic but different yield responses of C3 and C3 crops to elevated O3, Proc. Natl. Acad. Sci., 120, e2313591120, doi:10.1073/pnas.2313591120, 2023.

Li, X. and Xiao, J.: A Global, 0.05-Degree Product of Solar-Induced Chlorophyll Fluorescence Derived from OCO-2, MODIS, and Reanalysis Data, Remote Sens., 11, 10.3390/rs11050517, 2019.

Liang, S. L., Cheng, J., Jia, K., Jiang, B., Liu, Q., Xiao, Z. Q., Yao, Y. J., Yuan, W. P., Zhang, X. T., Zhao, X., and Zhou, J.: The Global Land Surface Satellite (GLASS) Product Suite, Bull. Amer. Meteorol. Soc., 102, E323-E337, 10.1175/bams-d-18-0341.1, 2021.

Lin, M., Horowitz, L. W., Xie, Y., Paulot, F., Malyshev, S., Shevliakova, E., Finco, A., Gerosa, G., Kubistin, D., and Pilegaard, K.: Vegetation feedbacks during drought exacerbate ozone air pollution extremes in Europe, Nat. Clim. Chang., 10, 444-+, 10.1038/s41558-020-0743-y, 2020.

Liu, X., Chu, B., Tang, R., Liu, Y., Qiu, B., Gao, M., Li, X., Xiao, J., Sun, H. Z., Huang, X., Desai, A. R., Ding, A., and Wang, H.: Air quality improvements can strengthen China's food security, Nat. Food, 10.1038/s43016-023-00882-y, 2024.

Liu, Y., Xue, Y., MacDonald, G., Cox, P., and Zhang, Z.: Global vegetation variability and its response to elevated CO2, global warming, and climate variability - a study using the offline SSiB4/TRIFFID model and satellite data, Earth Syst. Dynam., 10, 9-29, 10.5194/esd-10-9-2019, 2019.

Liu, Z., Zhou, M., Li, D., Song, T., Yue, X., Lu, X., Zhao, Y., and Zhang, L.: Co-benefit of forestation on ozone air quality and carbon storage in South China, Nat. Commun., 16, 2429, 10.1038/s41467-025-57548-5, 2025.

Lombardozzi, D., Levis, S., Bonan, G., Hess, P. G., and Sparks, J. P.: The Influence of Chronic Ozone Exposure on Global Carbon and Water Cycles, J. Clim., 28, 292-305, 10.1175/jcli-d-14-00223.1, 2015.

Long, X., Han, Y., Wang, Q. Y., Li, X. K., Feng, T., Wang, Y. C., Wang, Y., Zhang, S. L., Han, Y. M., Li, G. H., Tie, X. X., Cao, J. J., and Chen, Y.: Adverse Effects of Ozone Pollution on Net Primary Productivity in the North China Plain, Geophys. Res. Lett., 51, e2023GL105209, https://doi.org/10.1029/2023GL105209, 2024.

Lu, X., Hong, J., Zhang, L., Cooper, O. R., Schultz, M. G., Xu, X., Wang, T., Gao, M., Zhao, Y., and Zhang, Y.: Severe Surface Ozone Pollution in China: A Global Perspective, Environmental Science & Technology Letters, 5, 487-494, 10.1021/acs.estlett.8b00366, 2018.

Ma, Y., Yue, X., Sitch, S., Unger, N., Uddling, J., Mercado, L. M., Gong, C., Feng, Z., Yang, H., Zhou, H., Tian, C., Cao, Y., Lei, Y., Cheesman, A. W., Xu, Y., and Duran Rojas, M. C.: Implementation of trait-based ozone plant sensitivity in the

https://doi.org/10.5194/egusphere-2026-1335
Preprint. Discussion started: 18 March 2026

Yale Interactive terrestrial Biosphere model v1.0 to assess global vegetation damage, Geosci. Model Dev., 16, 2261-2276, 10.5194/gmd-16-2261-2023, 2023.

Monks, P. S., Archibald, A. T., Colette, A., Cooper, O., Coyle, M., Derwent, R., Fowler, D., Granier, C., Law, K. S., Mills, G. E., Stevenson, D. S., Tarasova, O., Thouret, V., von Schneidemesser, E., Sommariva, R., Wild, O., and Williams, M. L.: Tropospheric ozone and its precursors from the urban to the global scale from air quality to short-lived climate forcer, Atmos. Chem. Phys., 15, 8889-8973, 10.5194/acp-15-8889-2015, 2015.

Moreno-Martínez, Á., Camps-Valls, G., Kattge, J., Robinson, N., Reichstein, M., van Bodegom, P., Kramer, K., Cornelissen, J. H. C., Reich, P., Bahn, M., Niinemets, Ü., Peñuelas, J., Craine, J. M., Cerabolini, B. E. L., Minden, V., Laughlin, D. C., Sack, L., Allred, B., Baraloto, C., Byun, C., Soudzilovskaia, N. A., and Running, S. W.: A methodology to derive global maps of leaf traits using remote sensing and climate data, Remote Sens. Environ., 218, 69-88, 10.1016/j.rse.2018.09.006, 2018.

Munger, J. W., Wofsy, S. C., Bakwin, P. S., Fan, S.-M., Goulden, M. L., Daube, B. C., Goldstein, A. H., Moore, K. E., and Fitzjarrald, D. R.: Atmospheric deposition of reactive nitrogen oxides and ozone in a temperate deciduous forest and a subarctic woodland: 1. Measurements and mechanisms, Journal of Geophysical Research: Atmospheres, 101, 12639-12657, https://doi.org/10.1029/96JD00230, 1996.

Muñoz Sabater, J.: ERA5-Land hourly data from 1981 to present [dataset], https://doi.org/10.24381/cds.e2161bac, 2019.

Pleijel, H., Danielsson, H., and Broberg, M. C.: Benefits of the Phytotoxic Ozone Dose (POD) index in dose-response functions for wheat yield loss, Atmos. Environ., 268, 118797, https://doi.org/10.1016/j.atmosenv.2021.118797, 2022.

Reich, P. B.: Quantifying plant response to ozone: a unifying theory, Tree Physiol., 3, 63-91, 10.1093/treephys/3.1.63, 1987.

Ren, W., Tian, H., Tao, B., Chappelka, A., Sun, G., Lu, C., Liu, M., Chen, G., and Xu, X.: Impacts of tropospheric ozone and climate change on net primary productivity and net carbon exchange of China's forest ecosystems, Glob. Ecol. Biogeogr., 20, 391-406, https://doi.org/10.1111/j.1466-8238.2010.00606.x, 2011.

Scimone, G., Carucci, M. G., Risoli, S., Pisuttu, C., Cotrozzi, L., Lorenzini, G., Nali, C., Pellegrini, E., and Petersen, M.: Ozone Treatment as an Approach to Induce Specialized Compounds in Melissa officinalis Plants, Plants, 13, 933, 2024.

Sellers, P. J., Randall, D. A., Collatz, G. J., Berry, J. A., Field, C. B., Dazlich, D. A., Zhang, C., Collelo, G. D., and Bounoua, L.: A revised land surface parameterization (SiB2) for atmospheric GCMs .1. Model formulation, J. Clim., 9, 676-705, 10.1175/1520-0442(1996)009<0676:Arlspf>2.0.Co;2, 1996.

Sharma, P., Jha, A. B., Dubey, R. S., and Pessarakli, M.: Reactive Oxygen Species, Oxidative Damage, and Antioxidative Defense Mechanism in Plants under Stressful Conditions, Journal of Botany, 2012, 217037, https://doi.org/10.1155/2012/217037, 2012.

Sitch, S., Cox, P. M., Collins, W. J., and Huntingford, C.: Indirect radiative forcing of climate change through ozone effects on the land-carbon sink, Nature, 448, 791-U794, 10.1038/nature06059, 2007.

Tarasick, D., Galbally, I. E., Cooper, O. R., Schultz, M. G., Ancellet, G., Leblanc, T., Wallington, T. J., Ziemke, J., Liu, X., Steinbacher, M., Staehelin, J., Vigouroux, C., Hannigan, J. W., García, O., Foret, G., Zanis, P., Weatherhead, E.,

https://doi.org/10.5194/egusphere-2026-1335
Preprint. Discussion started: 18 March 2026

Petropavlovskikh, I., Worden, H., Osman, M., Liu, J., Chang, K.-L., Gaudel, A., Lin, M., Granados-Muñoz, M., Thompson, A. M., Oltmans, S. J., Cuesta, J., Dufour, G., Thouret, V., Hassler, B., Trickl, T., and Neu, J. L.: Tropospheric Ozone Assessment Report: Tropospheric ozone from 1877 to 2016, observed levels, trends and uncertainties, Elementa: Science of the Anthropocene, 7, 39, 10.1525/elementa.376, 2019.

Turnock, S. T., Allen, R. J., Andrews, M., Bauer, S. E., Deushi, M., Emmons, L., Good, P., Horowitz, L., John, J. G., Michou, M., Nabat, P., Naik, V., Neubauer, D., O'Connor, F. M., Olivié, D., Oshima, N., Schulz, M., Sellar, A., Shim, S., Takemura, T., Tilmes, S., Tsigaridis, K., Wu, T., and Zhang, J.: Historical and future changes in air pollutants from CMIP6 models, Atmos. Chem. Phys., 20, 14547-14579, 10.5194/acp-20-14547-2020, 2020.

Wang, T., Xue, L., Feng, Z., Dai, J., Zhang, Y., and Tan, Y.: Ground-level ozone pollution in China: a synthesis of recent findings on influencing factors and impacts, Environ. Res. Lett., 17, 10.1088/1748-9326/ac69fe, 2022.

Wang, Y. P., Lu, X. J., Wright, I. J., Dai, Y. J., Rayner, P. J., and Reich, P. B.: Correlations among leaf traits provide a significant constraint on the estimate of global gross primary production, Geophys. Res. Lett., 39, https://doi.org/10.1029/2012GL053461, 2012.

Wittig, V. E., Ainsworth, E. A., and Long, S. P.: To what extent do current and projected increases in surface ozone affect photosynthesis and stomatal conductance of trees? A meta-analytic review of the last 3 decades of experiments, Plant Cell Environ., 30, 1150-1162, 10.1111/j.1365-3040.2007.01717.x, 2007.

Xie, X. D., Wang, T. J., Yue, X., Li, S., Zhuang, B. L., Wang, M. H., and Yang, X. Q.: Numerical modeling of ozone damage to plants and its effects on atmospheric CO2 in China, Atmos. Environ., 217, 10.1016/j.atmosenv.2019.116970, 2019.

Yue, X. and Unger, N.: Ozone vegetation damage effects on gross primary productivity in the United States, Atmos. Chem. Phys., 14, 9137-9153, 10.5194/acp-14-9137-2014, 2014.

Yue, X., Unger, N., Harper, K., Xia, X., Liao, H., Zhu, T., Xiao, J., Feng, Z., and Li, J.: Ozone and haze pollution weakens net primary productivity in China, Atmos. Chem. Phys., 17, 6073-6089, 10.5194/acp-17-6073-2017, 2017.

Zhan, X. W., Xue, Y. K., and Collatz, G. J.: An analytical approach for estimating CO2 and heat fluxes over the Amazonian region, Ecol. Model., 162, 97-117, 10.1016/s0304-3800(02)00405-2, 2003.

Zhang, H., Liu, D., Dong, W., Cai, W., and Yuan, W.: Accurate representation of leaf longevity is important for simulating ecosystem carbon cycle, Basic Appl. Ecol., 17, 396-407, https://doi.org/10.1016/j.baae.2016.01.006, 2016.

Zhang, W., Liu, D., Tian, H., Pan, N., Yang, R., Tang, W., Yang, J., Lu, F., Dayananda, B., Mei, H., Wang, S., and Shi, H.: Parsimonious estimation of hourly surface ozone concentration across China during 2015–2020, Sci. Data, 11, 492, 10.1038/s41597-024-03302-3, 2024.

Zhang, Z., Xue, Y., MacDonald, G., Cox, P. M., and Collatz, G. J.: Investigation of North American vegetation variability under recent climate: A study using the SSiB4/TRIFFID biophysical/dynamic vegetation model, J. Geophys. Res.-Atmos., 120, 1300-1321, 10.1002/2014jd021963, 2015.

Zhou, H., Yue, X., Dai, H., Geng, G., Yuan, W., Chen, J., Shen, G., Zhang, T., Zhu, J., and Liao, H.: Recovery of ecosystem productivity in China due to the Clean Air Action plan, Nat. Geosci., 10.1038/s41561-024-01586-z, 2024.

https://doi.org/10.5194/egusphere-2026-1335
Preprint. Discussion started: 18 March 2026

Zhu, J., Tai, A. P. K., and Hung Lam Yim, S.: Effects of ozone–vegetation interactions on meteorology and air quality in China using a two-way coupled land–atmosphere model, Atmos. Chem. Phys., 22, 765-782, 10.5194/acp-22-765-2022, 2022.